Joint Delay-Doppler Estimation Performance in a Dual Source Context

Corentin Lubeigt, Lorenzo Ortega, Jordi Vilà-Valls, Laurent Lestarquit, Eric Chaumette

remote sensing

MDPI

Article

Joint Delay-Doppler Estimation Performance in a Dual Source Context

Corentin Lubeigt [1,2,*], Lorenzo Ortega [1,2], Jordi Vilà-Valls [2], Laurent Lestarquit [3] and Eric Chaumette [2]

1 Telecommunication for Space and Aeronautics (TéSA) Laboratory, 31500 Toulouse, France; lorenzo.ortega@tesa.prd.fr
2 ISAE-SUPAERO, University of Toulouse, 31400 Toulouse, France; jordi.vila-valls@isae-supaero.fr (J.V.-V.); eric.chaumette@isae-supaero.fr (E.C.)
3 CNES, 31400 Toulouse, France; laurent.lestarquit@cnes.fr
* Correspondence: corentin.lubeigt@tesa.prd.fr

Received: 20 October 2020; Accepted: 24 November 2020; Published: 27 November 2020

Abstract: Evaluating the time-delay, Doppler effect and carrier phase of a received signal is a challenging estimation problem that was addressed in a large variety of remote sensing applications. This problem becomes more difficult and less understood when the signal is reflected off one or multiple surfaces and interferes with itself at the receiver stage. This phenomenon might deteriorate the overall system performance, as for the multipath effect in Global Navigation Satellite Systems (GNSS), and mitigation strategies must be accounted for. In other applications such as GNSS reflectometry (GNSS-R) it may be interesting to estimate the parameters of the reflected signal to deduce the geometry and the surface characteristics. In either case, a better understanding of this estimation problem is directly brought by the corresponding lower performance bounds. In the high signal-to-noise ratio regime of the Gaussian conditional signal model, the Cramér-Rao bound (CRB) provides an accurate lower bound in the mean square error sense. In this article, we derive a new compact CRB expression for the joint time-delay and Doppler estimation in a dual source context, considering a band-limited signal and its specular reflection. These compact CRBs are expressed in terms of the baseband signal samples, making them especially easy to use whatever the baseband signal considered, therefore being valid for a variety of remote sensors. This extends existing results in the single source context and opens the door to a plethora of usages to be discussed in the article. The proposed CRB expressions are validated in two representative navigation and radar examples.

Keywords: time-delay and Doppler estimation; Cramér-Rao bound; maximum likelihood; band-limited signals; dual source; GNSS multipath; GNSS remote sensing

1. Introduction

The joint delay-Doppler estimation problem has been addressed for years as it is a key step in a plethora of applications such as radar, sonar, communications, navigation or remote sensing [1–7]. For instance, this estimation is performed by a receiver in order to localize and track the position of sources such as a transmitting satellite, like in Global Navigation Satellite System (GNSS), or a radiated target from which the system receives the backscattered signal. Under nominal conditions the receiver collects only line-of-sight (LOS) signals. However, in challenging realistic scenarios like urban canyons, extended targets or in conventional reflectometry configurations, a series of non-line-of-sight (NLOS) echoes may be collected by the receiver. Those echoes, often referred to as multipath, are usually the consequence of good enough reflecting surfaces that are radiated by the sources of interest, which in turn reach the receiver on top of the LOS signals.

In some applications the user tries to mitigate the multipath effect because it tends to degrade the quality of the LOS signals of interest, directly affecting the overall system performance. This is the case in standard GNSS where numerous techniques were developed to get rid of the multipath interference (e.g., MEDLL [8], MMT [9], Vision Correlator [10]). Indeed, GNSS multipath remains one of the main sources of error in challenging urban environments, therefore being a key point to be addressed for safety-critical applications requiring a precise receiver position, such as in intelligent transportation systems. In other applications the user wants to collect and exploit such interference in order to extract features related to the secondary propagation medium or the reflecting surface properties. A typical example is GNSS reflectometry (GNSS-R) where the secondary signal is the main source of information. In GNSS-R, a first approach is to have two separated antennas: one pointing upward collecting the LOS signal and the other one pointing downward, collecting the reflected signal [11,12]. A second approach is to collect both signals with a single antenna and process the resulting superimposed signals [13,14]. Both GNSS multipath (i.e., considering one LOS signal and a main secondary path contribution) and the single antenna GNSS-R approach are typical scenarios of a dual source estimation problem, being the main problem of interest in this contribution.

When it comes to the estimation of deterministic parameters (i.e., such as time-delay and Doppler in this contribution), a powerful tool to determine the best statistical performance are Cramér-Rao Bounds (CRBs). Indeed, these bounds accurately describe the ultimate achievable minimum variance that an unbiased estimator can reach for a given problem. The CRBs for the delay and delay-Doppler estimation have been investigated in several contributions for different signal models, considering signals with a finite [1,15–18] or infinite [19] bandwidth. Regarding the contributions dealing with finite bandwidth signals it is common to resort to the narrowband signal assumption, that is, the impact of the Doppler effect on the baseband signal is neglected and only amounts to a time-varying frequency shift [20]. The derivation of such bounds are often based on the Slepian-Bangs formulas [21] or more general theoretical expressions for Gaussian observation models [22–24]. When considering a multiple source signal model the CRB derivation complexity increases significantly. Examples of those CRB expressions were derived for the case of extended targets [25] and in GNSS-R for altimetry purposes [26–28]. Despite these contributions, a dual source delay-Doppler estimation compact closed-form CRB expression for generic band-limited signals is not available in the literature, being an important missing point and a result of broad interest.

In either the single or multiple source context, the problem can be formulated as a Conditional Signal Model (CSM) [16–18,29–33]. Such model and the corresponding Conditional Maximum Likelihood Estimator (CMLE) lead to interesting properties: the CMLE performance is accurately described by the CRB in the asymptotic region of operation, i.e., it is efficient in the high signal-to-noise ratio (SNR) regime and/or the large sample regime [29,34]. This makes the CMLE an interesting tool to validate CRB expressions, as done for instance in [16–18,35]. Unfortunately, the main CMLEs drawback is their heavy computational load, which the practitioner usually wants to avoid, and therefore many solutions to reduce this load were proposed in the literature. A first approach consists in using sub-optimal techniques, where the multidimensional search is substituted with a simpler one-dimensional one, such as in the Capon [36] or MUSIC [37,38] methods. Another approach is to reduce the computational burden by splitting the multidimensional optimization search in a number of recursive searches. The Alternating Projection algorithm [39] and the relaxed version of the CLEAN algorithm [40] are two well-known examples of this approach.

1.1. Contributions

Keeping in mind the problem of interest, that is, the dual source delay-Doppler estimation with a generic band-limited signal, the main contributions of this article are as follows:

- A compact Fisher Information Matrix (FIM) for the general dual source narrowband CSM (i.e., where the Doppler effect on the band-limited baseband signal is not considered and amounts to a frequency shift) is provided in Section 3. This extends the work of [17,18] dealing with the

single source narrowband CSM and completes the work of [28] in which the FIM is given for the specific case of a static, ground-based receiver, leading yo an identical Doppler effect for the two paths;
- The FIM is expressed in an easy to use form, based on the baseband signal samples;
- The theoretical results are supported and validated by the implementation of a dual source CMLE [1] and sub-optimal estimators such as a CLEAN RELAX Estimator (CRE) [40];
- The formal connection with existing literature [28] and possible uses of the new CRB are discussed;

1.2. Notation

The notation adopted is as follows: scalars are represented by italic lowercase characters as in b, vectors are represented by bold lowercase characters as in $\mathbf{b}$, and matrices are represented by bold uppercase characters as in $\mathbf{B}$. The transpose operation is indicated by the superscript ^{T}, the conjugate transpose by the superscript ^{H}, and the conjugate operation by the superscript *. $\mathbf{I}_n$ represents the identity matrix of dimension n, $\mathrm{Re}\{\cdot\}$ and $\mathrm{Im}\{\cdot\}$ refer to the real part and the imaginary part.

1.3. Organization

Section 2 provides details on the context and the corresponding narrowband signal model. In Section 3 the CRB derivation is presented for the delay, Doppler, amplitude and phase estimation of a band-limited signal in the dual source context. Section 4 introduces the CMLE and a sub-optimal estimator. These two estimators are used to validate the new CRBs. Section 5 provides results for two representative examples. Section 6.1 relates the presented results to the literature and Section 6.2 gives an overview of how the current study can branch out into specific studies. Finally a conclusion is drawn in Section 7.

2. Signal Model

2.1. Single Antenna Receiver

In order to study the dual source problem we consider a receiver with a single antenna able to collect both a LOS signal (signal labelled 0) and a single NLOS reflection (signal labelled 1), which may be reflected for instance in a ground, sea or building surface (see Figure 1). Here we assume a purely specular reflection with no scattering effect as considered in [28,41]. Note that this model is also related to the multipath model used in the GNSS literature ((6.42) [42]).

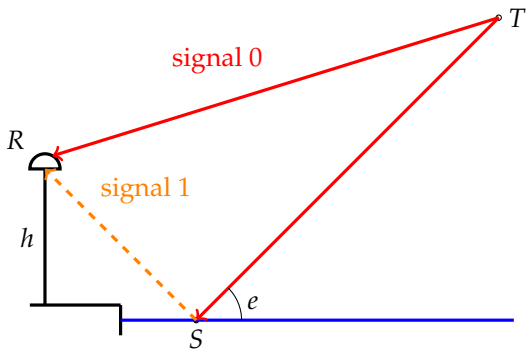

Figure 1. Geometry of the problem, with h the altitude of the receiver and e the elevation angle of the transmitter seen from the specular point.

We consider that a transmitter T and a receiver R have uniform linear motions such that the positions can be described as $\mathbf{p}_T(t) = \mathbf{p}_T + \mathbf{v}_T t$ and $\mathbf{p}_R(t) = \mathbf{p}_R + \mathbf{v}_R t$, where $\mathbf{p}$ and $\mathbf{v}$ are the position and velocity vectors, respectively and t is the time. Under such conditions, the distance between T and R can be approximated by a first order distance-velocity model [20]:

$$\|\mathbf{p}_{TR}(t)\| \triangleq \|\mathbf{p}_R(t) - \mathbf{p}_T(t - \tilde{\tau}(t))\| = c\tilde{\tau}(t) \approx d + vt, \text{ and } \tilde{\tau}(t) \approx \tau + bt,\ \tau = \frac{d}{c},\ b = \frac{v}{c}, \quad (1)$$

where d is the absolute distance between T and R, v is the radial velocity between T and R, τ is the time-delay due to the propagation path and $(1-b)$ is the dilatation induced by the Doppler effect and c the speed of light in vacuum.

2.2. Narrowband Signal Model

A band-limited signal $s(t)$, with bandwidth B, transmitted over a carrier frequency f_c ($\lambda_c = c/f_c$) is considered in this study. This signal can be expressed as

$$s(t) = \sum_{n=N_1'}^{N_2'} s\left(\frac{n}{F_s}\right) \text{sinc}\left(\pi F_s\left(t - \frac{n}{F_s}\right)\right) \leftrightharpoons S(f) = \frac{1}{F_s}\sum_{n=N_1'}^{N_2'} s\left(\frac{n}{F_s}\right) e^{-j2\pi n\frac{f}{F_s}},\ -\frac{F_s}{2} \leq f \leq \frac{F_s}{2}, \quad (2)$$

where sinc$(\cdot)$ is the sine cardinal function, f is the frequency, $F_s \geq B$ is the sampling frequency, $N_1', N_2' \in \mathbb{Z}^2$, $N_1' < N_2'$ and $\leftrightharpoons$ refers to the time-frequency pair that will be helpful for the bounds derivation. Using (1), the dual source complex analytic signal at the output of the receiver's antenna can be expressed as

$$\begin{aligned} x_R(t) &= d_R(t;\boldsymbol{\eta}_0,\rho_0,\phi_{R,0}) + d_R(t;\boldsymbol{\eta}_1,\rho_1,\phi_{R,1}) + w_R(t), \\ d_R(t;\boldsymbol{\eta}_i,\rho_i,\phi_{R,i}) &= \rho_i e^{j\phi_{R,i}} s((1-b_i)(t-\tau_i)) e^{j\omega_c(1-b_i)t} e^{-j\omega_c\tau_i}, \end{aligned}$$

where $w_R(t)$ is a zero-mean white complex circular Gaussian noise, $\omega_c = 2\pi f_c$, and for $i \in \{0,1\}$, $\boldsymbol{\eta}_i^T = [\tau_i, b_i]$, $\rho_i \in]0,+\infty[$ and $\phi_{R,i}$ the amplitude and phase of the complex coefficients induced by the propagation characteristics (fading, reflection, etc.), the polarization mismatches and the antenna gains.

Under the narrowband signal hypothesis, i.e., the time-frequency product $B \cdot T_c$ (with B the signal bandwidth and T_c the coherent integration time) is smaller than the inverse Doppler term c/v, the Doppler effect on the band-limited baseband signal $s(t)$ is usually neglected so that: $s((1-b)(t-\tau)) \approx s(t-\tau)$ (ch.9 [1]). Therefore, the baseband output of the receiver's Hilbert filter with bandwidth F_s containing a direct signal and a single specular reflection can be approximated by

$$x(t) \triangleq x_R(t)e^{-j\omega_c t} = d(t;\boldsymbol{\theta}_0) + d(t;\boldsymbol{\theta}_1) + w(t)\ , \quad (3)$$

$$d(t;\boldsymbol{\theta}_i) \triangleq \rho_i e^{j\phi_i} s(t-\tau_i) e^{-j\omega_c b_i(t-\tau_i)}\ , \quad (4)$$

where for $i \in \{0,1\}$, $\boldsymbol{\theta}_i^T = [\boldsymbol{\eta}_i^T, \rho_i, \phi_i]$, $\phi_i = \phi_{R,i} - \omega_c(1+b_i)\tau_i$. If we now consider the acquisition of $N = N_2 - N_1 + 1$ ($N_1 \ll N_1', N_2 \gg N_2'$) samples at a sampling rate $T_s = 1/F_s$, the discrete signal model yields to the following dual source CSM,

$$\mathbf{x} = \mathbf{A}(\boldsymbol{\eta}_0,\boldsymbol{\eta}_1)\boldsymbol{\alpha} + \mathbf{w},\ \mathbf{w} \sim \mathcal{CN}(0,\sigma_n^2\mathbf{I}_N)\ , \quad (5)$$

with, for $n \in [N_1, N_2]$,

$$\begin{aligned} \mathbf{x}^T &= (\ldots,\ x(nT_s),\ \ldots)\ , \\ \mathbf{A}(\boldsymbol{\eta}_0,\boldsymbol{\eta}_1) &= [\mathbf{a}_0,\ \mathbf{a}_1]\ , \\ \mathbf{a}_i^T &= \left(\ldots,\ s(nT_s-\tau_i)e^{-j\omega_c b_i(nT_s-\tau_i)},\ \ldots\right)\ , \\ \boldsymbol{\alpha}^T &= \left(\rho_0 e^{j\phi_0},\ \rho_1 e^{j\phi_1}\right)\ , \\ \mathbf{w}^T &= (\ldots,\ w(nT_s),\ \ldots)\ . \end{aligned}$$

3. New Compact Dual Source CRB for Delay and Doppler Estimation with Band-Limited Signals

The main goal of this contribution is to derive a new compact analytic form of the delay-Doppler CRB for the dual source model in (5).

3.1. Problem Formulation

The parameters to be estimated are gathered in the following vector: $\boldsymbol{\epsilon}^T = [\sigma_n^2, \boldsymbol{\eta}_0^T, \rho_0, \phi_0, \boldsymbol{\eta}_1^T, \rho_1, \phi_1]$. From (5), we can write $\mathbf{x} \sim \mathcal{CN}\left(\mathbf{A}(\boldsymbol{\eta}_0, \boldsymbol{\eta}_1)\boldsymbol{\alpha}, \sigma_n^2 \mathbf{I}_N\right)$ and express the probability density function (pdf) as,

$$p(\mathbf{x}, \boldsymbol{\epsilon}) = \frac{1}{(\pi\sigma_n^2)^N} e^{-\frac{1}{\sigma_n^2}\|\mathbf{x}-\mathbf{A}(\boldsymbol{\eta}_0,\boldsymbol{\eta}_1)\boldsymbol{\alpha}\|^2} . \tag{6}$$

The corresponding CRB for the estimation of $\boldsymbol{\epsilon}$ is defined as the inverse of the Fisher Information matrix (FIM) [43],

$$\mathbf{CRB}_{\boldsymbol{\epsilon}|\boldsymbol{\epsilon}} = \mathbf{F}_{\boldsymbol{\epsilon}|\boldsymbol{\epsilon}}^{-1}(\boldsymbol{\epsilon}),\ \mathbf{F}_{\boldsymbol{\epsilon}|\boldsymbol{\epsilon}}(\boldsymbol{\epsilon}) = -E\left[\frac{\partial^2 \ln p(\mathbf{x}, \boldsymbol{\epsilon})}{\partial\boldsymbol{\epsilon}\partial\boldsymbol{\epsilon}^T}\right] . \tag{7}$$

Note that for the Gaussian CSM of interest the Slepian-Bangs formula [21] provides the direct evaluation of the FIM terms,

$$\left(\boldsymbol{F}_{\boldsymbol{\epsilon}|\boldsymbol{\epsilon}}\left(\boldsymbol{\epsilon}\right)\right)_{k,l} \triangleq F_{\epsilon_k,\epsilon_l|\boldsymbol{\epsilon}}\left(\boldsymbol{\epsilon}\right) = \frac{2}{\sigma_n^2}\mathrm{Re}\left\{\left(\frac{\partial\mathbf{A}\boldsymbol{\alpha}}{\partial\epsilon_k}\right)^H\left(\frac{\partial\mathbf{A}\boldsymbol{\alpha}}{\partial\epsilon_l}\right)\right\} + \frac{N}{\sigma_n^4}\frac{\partial\sigma_n^2}{\partial\epsilon_k}\frac{\partial\sigma_n^2}{\partial\epsilon_l} , \tag{8}$$

where the noise power appears to be independent from the other parameters, and the FIM reduces to

$$\mathbf{F}_{\boldsymbol{\epsilon}|\boldsymbol{\epsilon}}(\boldsymbol{\epsilon}) = \begin{bmatrix} F_{\sigma_n^2|\boldsymbol{\epsilon}}(\boldsymbol{\epsilon}) & \mathbf{0} & \mathbf{0} \\ \mathbf{0} & \mathbf{F}_{\boldsymbol{\theta}_0|\boldsymbol{\epsilon}}(\boldsymbol{\epsilon}) & \mathbf{F}_{\boldsymbol{\theta}_0,\boldsymbol{\theta}_1|\boldsymbol{\epsilon}}(\boldsymbol{\epsilon}) \\ \mathbf{0} & \mathbf{F}_{\boldsymbol{\theta}_1,\boldsymbol{\theta}_0|\boldsymbol{\epsilon}}(\boldsymbol{\epsilon}) & \mathbf{F}_{\boldsymbol{\theta}_1|\boldsymbol{\epsilon}}(\boldsymbol{\epsilon}) \end{bmatrix} , \tag{9}$$

where:

- $F_{\sigma_n^2|\boldsymbol{\epsilon}}(\boldsymbol{\epsilon}) = N/\sigma_n^4$.
- $\mathbf{F}_{\boldsymbol{\theta}_0|\boldsymbol{\epsilon}}(\boldsymbol{\epsilon})$ and $\mathbf{F}_{\boldsymbol{\theta}_1|\boldsymbol{\epsilon}}(\boldsymbol{\epsilon})$ correspond to the FIMs of the signals when they are totally decoupled. These matrices have been derived and studied in [16] without the Doppler frequency estimation, and in [17,18] for the general Gaussian CSM. The main results in [17,18] concerning the single source CSM FIM terms are summarized in Section 3.2.
- $\mathbf{F}_{\boldsymbol{\theta}_0,\boldsymbol{\theta}_1|\boldsymbol{\epsilon}}(\boldsymbol{\epsilon}) = \mathbf{F}_{\boldsymbol{\theta}_1,\boldsymbol{\theta}_0|\boldsymbol{\epsilon}}(\boldsymbol{\epsilon})^T$ characterizes the interference between both signals. The derivation of such FIM terms is given in Section 3.3.

3.2. Decoupled Fisher Information Matrix Terms

The two last diagonal blocks of the FIM (9) were derived for the single source CSM case in [17,18]. For the sake of completeness, the main results are recalled in the sequel:

$$\mathbf{F}_{\boldsymbol{\theta}_i|\boldsymbol{\epsilon}}(\boldsymbol{\epsilon}) = \frac{2F_s}{\sigma_n^2}\mathrm{Re}\left\{\mathbf{Q}_i\mathbf{W}\mathbf{Q}_i^H\right\} , \tag{10}$$

where $\mathbf{Q}_i$, $i \in \{1, 2\}$ is defined in (A9) and $\mathbf{W}$ is defined as:

$$\mathbf{W} = \begin{bmatrix} w_1 & w_2^* & w_3^* \\ w_2 & W_{2,2} & w_4^* \\ w_3 & w_4 & W_{3,3} \end{bmatrix} , \tag{11}$$

with the easy-to-use formulation w.r.t. the baseband signal samples:

$$w_1 = \frac{1}{F_s}\mathbf{s}^H\mathbf{s},\ w_2 = \frac{1}{F_s^2}\mathbf{s}^H\mathbf{D}\mathbf{s},\ w_3 = \mathbf{s}^H\mathbf{V}^{\Delta,1}(0)\mathbf{s},\ w_4 = \frac{1}{F_s}\mathbf{s}^H\mathbf{D}\mathbf{V}^{\Delta,1}(0)\mathbf{s},$$
$$W_{2,2} = \frac{1}{F_s^3}\mathbf{s}^H\mathbf{D}^2\mathbf{s},\ W_{3,3} = F_s\mathbf{s}^H\mathbf{V}^{\Delta,2}(0)\mathbf{s}, \tag{12}$$

where $\mathbf{s}$, the baseband sample vector, is defined in (A36), $\mathbf{D}$ in (A39), $\mathbf{V}^{\Delta,1}$ in (A41) and $\mathbf{V}^{\Delta,2}$ in (A42). The inversion of (10) proposed in [17,18] leads to a closed-form CRB expression for the delay, Doppler, phase and amplitude estimation, where a noteworthy feature is that the CRBs are expressed w.r.t. the baseband signal samples. Such CRBs were studied for different GNSS signals in [35,44].

3.3. Interference Fisher Information Matrix Terms

From the Slepian-Bangs formula the non-diagonal blocks of the FIM, referred to as interference Fisher information matrices, are expressed as follows:

$$\mathbf{F}_{\boldsymbol{\theta}_1,\boldsymbol{\theta}_0|\boldsymbol{\epsilon}}(\boldsymbol{\epsilon}) = \frac{2F_s}{\sigma_n^2}\mathrm{Re}\left\{\mathbf{Q}_1\mathbf{W}^{\Delta}\mathbf{Q}_0^H\right\}, \tag{13}$$

where $\mathbf{Q}_0$, $\mathbf{Q}_1$ are defined in (A9) and $\mathbf{W}^{\Delta}$ is defined as

$$\mathbf{W}^{\Delta} = \begin{bmatrix} W_{1,1}^{\Delta} & W_{1,2}^{\Delta} & W_{1,3}^{\Delta} \\ W_{2,1}^{\Delta} & W_{2,2}^{\Delta} & W_{2,3}^{\Delta} \\ W_{3,1}^{\Delta} & W_{3,2}^{\Delta} & W_{3,3}^{\Delta} \end{bmatrix} e^{j\Delta\psi}e^{-j\omega_c\Delta b\tau_0}, \tag{14}$$

where Δb and $\Delta\psi$ are defined in (A15) and with the different components of the matrix $\mathbf{W}^{\Delta}$ expressed w.r.t the baseband signal samples given by

$$W_{1,1}^{\Delta} = \frac{1}{F_s}\mathbf{s}^H\mathbf{U}(\Delta b)\mathbf{V}^{\Delta,0}\left(\frac{\Delta\tau}{T_s}\right)\mathbf{s}, \tag{15}$$
$$W_{1,2}^{\Delta} = \frac{1}{F_s^2}\mathbf{s}^H\mathbf{D}\mathbf{U}(\Delta b)\mathbf{V}^{\Delta,0}\left(\frac{\Delta\tau}{T_s}\right)\mathbf{s}, \tag{16}$$
$$W_{1,3}^{\Delta} = -\mathbf{s}^H\mathbf{U}(\Delta b)\mathbf{V}^{\Delta,1}\left(\frac{\Delta\tau}{T_s}\right)\mathbf{s} + \frac{j\omega_c\Delta b}{F_s}\mathbf{s}^H\mathbf{U}(\Delta b)\mathbf{V}^{\Delta,0}\mathbf{s}, \tag{17}$$
$$W_{2,1}^{\Delta} = \frac{1}{F_s^2}\mathbf{s}^H\mathbf{U}(\Delta b)\mathbf{V}^{\Delta,0}\left(\frac{\Delta\tau}{T_s}\right)\mathbf{D}\mathbf{s}, \tag{18}$$
$$W_{2,2}^{\Delta} = \frac{1}{F_s^3}\mathbf{s}^H\mathbf{D}\mathbf{U}(\Delta b)\mathbf{V}^{\Delta,0}\left(\frac{\Delta\tau}{T_s}\right)\mathbf{D}\mathbf{s}, \tag{19}$$
$$W_{2,3}^{\Delta} = -\frac{1}{F_s}\mathbf{s}^H\mathbf{U}(\Delta b)\mathbf{V}^{\Delta,1}\left(\frac{\Delta\tau}{T_s}\right)\mathbf{D}\mathbf{s} + \frac{j\omega_c\Delta b}{F_s^2}\mathbf{s}^H\mathbf{U}(\Delta b)\mathbf{V}^{\Delta,0}\left(\frac{\Delta\tau}{T_s}\right)\mathbf{D}\mathbf{s}, \tag{20}$$
$$W_{3,1}^{\Delta} = \mathbf{s}^H\mathbf{U}(\Delta b)\mathbf{V}^{\Delta,1}\left(\frac{\Delta\tau}{T_s}\right)\mathbf{s}, \tag{21}$$
$$W_{3,2}^{\Delta} = \frac{1}{F_s}\mathbf{s}^H\mathbf{D}\mathbf{U}(\Delta b)\mathbf{V}^{\Delta,1}\left(\frac{\Delta\tau}{T_s}\right)\mathbf{s}, \tag{22}$$
$$W_{3,3}^{\Delta} = F_s\mathbf{s}^H\mathbf{U}(\Delta b)\mathbf{V}^{\Delta,2}\left(\frac{\Delta\tau}{T_s}\right)\mathbf{s} + j\omega_c\Delta b\mathbf{s}^H\mathbf{U}(\Delta b)\mathbf{V}^{\Delta,1}\left(\frac{\Delta\tau}{T_s}\right)\mathbf{s}, \tag{23}$$

where $\mathbf{s}$, the baseband sample vector, is defined in (A36), $\mathbf{D}$ in (A39), $\mathbf{U}$ in (A38), $\mathbf{V}^{\Delta,0}$ in (A40), $\mathbf{V}^{\Delta,1}$ in (A41) and $\mathbf{V}^{\Delta,2}$ in (A42).

Proof. refer to Appendix A. □

An interesting and reassuring fact is that when the difference between LOS and NLOS signals (i.e., signal 0 and signal 1) is set to zero: $\Delta\tau = \tau_1 - \tau_0 = 0$, $\Delta b = b_1 - b_0 = 0$, $\Delta\phi = \phi_1 - \phi_0 = 0$, $\rho_1 = \rho_0$, we have $\mathbf{Q}_0 = \mathbf{Q}_1$ and $\mathbf{W}^{\Delta} = \mathbf{W}$. This result could be expected but the FIM terms equations

obtained confirm it. Indeed, if both signals are indistinguishable, they must have the same FIM and their interference FIM must coincide (total interference between both signals).

4. Maximum Likelihood and CLEAN RELAX Estimators

4.1. Dual Source Conditional Maximum Likelihood Estimator

From the dual source CSM (5) and its pdf (6), the estimator $\widehat{\boldsymbol{\epsilon}}$ that maximizes the likelihood is such that $(\widehat{\eta_0}, \widehat{\eta_1})$ maximizes the projection of the received signal onto the subspace defined by the mixing matrix $\mathbf{A}$ [22]. As a consequence, the estimated parameters $(\widehat{\rho_0}, \widehat{\rho_1}, \widehat{\phi_0}, \widehat{\phi_1})$ directly depend on the delay/Doppler estimation. Finally, $\widehat{\sigma_n^2}$ is simply the orthogonal projection value:

$$(\widehat{\eta_0}, \widehat{\eta_1}) = \arg\max_{\eta_0, \eta_1} \left\| \mathbf{P}_{\mathbf{A}(\eta_0, \eta_1)} \mathbf{x} \right\|^2 \tag{24}$$

$$\widehat{\rho_i} = \left| \left[\left(\mathbf{A}^H(\widehat{\eta_0}, \widehat{\eta_1}) \mathbf{A}(\widehat{\eta_0}, \widehat{\eta_1}) \right)^{-1} \mathbf{A}^H(\widehat{\eta_0}, \widehat{\eta_1}) \mathbf{x} \right]_i \right| \tag{25}$$

$$\widehat{\phi_i} = \arg \left\{ \left[\left(\mathbf{A}^H(\widehat{\eta_0}, \widehat{\eta_1}) \mathbf{A}(\widehat{\eta_0}, \widehat{\eta_1}) \right)^{-1} \mathbf{A}^H(\widehat{\eta_0}, \widehat{\eta_1}) \mathbf{x} \right]_i \right\} \tag{26}$$

$$\widehat{\sigma_n^2} = \frac{1}{N} \left\| \mathbf{P}^{\perp}_{\mathbf{A}(\eta_0, \eta_1)} \mathbf{x} \right\|^2 \tag{27}$$

where the projectors are defined as $\mathbf{P}_{\mathbf{A}} = \mathbf{A} \left(\mathbf{A}^H \mathbf{A} \right)^{-1} \mathbf{A}^H$, $\mathbf{P}^{\perp}_{\mathbf{A}} = \mathbf{I} - \mathbf{P}_{\mathbf{A}}$.

Even though this estimator is known to be computationally complex, it is also known to be asymptotically efficient (e.g., in the high-SNR regime [34]) for the dual source Gaussian CSM. This property makes it a powerful tool to validate the CRBs derived in Section 3.

4.2. Sub-Optimal Estimator: CLEAN-RELAX

In order to deal with the CMLE heavy computational load, alternative estimators can be used. In this paper, a relax version of the well-known CLEAN algorithm was implemented [40]. This estimator assumes that the two signals are decoupled. The method first estimates the parameters $(\widehat{\tau_0}, \widehat{b_0}, \widehat{\rho_0}, \widehat{\phi_0})$ of the strongest signal by using the cross-correlation function, it subtracts this estimated signal from the measured input, and then estimates the secondary signal parameters $(\widehat{\tau_1}, \widehat{b_1}, \widehat{\rho_1}, \widehat{\phi_1})$. These two estimation steps are iterated until the cost function, which is the resulting likelihood, is stabilized. The method used in this contribution only looks for two signals. In GNSS, the same algorithm is named Multipath Estimating Delay Lock Loop (MEDLL) and is typically used to mitigate multipath [8]. The CRE can be seen as a sub-optimal estimator because it works only under certain assumptions. Indeed, considering that the two signals can be decoupled stands only when $\Delta\tau$ is large enough compared to the sharpness of the cross-correlation function. This estimator is not expected to perform well when the two signals are very close in time. On the other hand, when the signals are clearly parted, the CRE asymptotically behaves as the CMLE. See Section 5 for simulated results on the CRE limit.

5. Validation and Discussion

5.1. Methodology

To validate the new CRBs derived in Section 3, the asymptotic properties of the CMLE introduced in Section 4.1 are exploited. It is know that for a high SNR the statistical mean square error (MSE) of the delay and Doppler frequency CMLE are accurately described by the corresponding CRBs. Two representative signals are considered: (i) a Global Positioning System (GPS) L1 C/A signal [45], and (ii) a Linear Frequency Modulated (LFM) chirp signal classically defined as following:

$$s(t) = e^{j2\pi f(t)},\ f(t) = \frac{B}{2T}\left(\frac{t}{T} - \frac{1}{2}\right)^2,\ T = NT_s, \tag{28}$$

with B the chirp bandwidth equal to 8 MHz (which is the receiver bandwidth in this case) and N the number of samples. The received signal is built with two delayed and attenuated replicas with arbitrary values of Doppler frequencies. The parameters for the three different scenarios considered are given in Table 1. Notice that the L1 C/A chips unit is 1/1023 ms. In this table ρ_1/ρ_0 is the ratio between the reflected amplitude and the main one (also referred to as multipath-to-direct ratio in GNSS [42]) and $F_{di} = b_i f_c$ refers to the Doppler frequency in Hertz corresponding to the Doppler stretch b_i.

As discussed in Section 4, depending on the time-delay difference between the two replicas, $\Delta\tau$, one can apply a sub-optimal estimators such as the CRE [40], which may behave like a CMLE in the asymptotic region (high SNR). In this case it is possible to see the estimator threshold region in a reasonable computation time. However, when it comes to very small values of $\Delta\tau$, meaning less than $1/F_s$ chip delay, a sub-optimal algorithm like the CRE is in general not able to converge to the CRB. As a consequence, during the simulations, when the product $\Delta\tau F_s$ is smaller than or equal to 1, the CRE is no longer efficient. In such limit case, a direct implementation of the CMLE is preferred. Computational cost soars but at very high-SNR it is possible to limit the search area at 3σ, where σ is the expected variance of the estimated values, directly provided by the derived CRBs. Therefore the CMLE simulation is valid only at very high SNR, because in this asymptotic region the CMLE is Gaussian distributed and its variance is equal to the CRB.

Table 1. Simulations scenarios for the CRB validation: (a) two signals totally parted ($\Delta\tau = 2$ chips), (b) a secondary path very close to the main signal ($\Delta\tau = 1/4$ chip), and (c) considered to showcase the difference between the CMLE and CRE ($\Delta\tau = 1/8$ chip).

	Estimator	F_s (MHz)	$\Delta\tau$ (L1 C/A Chips)	$\Delta\tau$ (m)	ρ_1/ρ_0	$\Delta\phi$ (°)	Fd_0/Fd_1 (Hz)
(a)	CRE	8	2	600	0.5	15	20/50
(b)	CRE	8	1/4	75	0.5	15	20/50
(c1)	CRE	8	1/8	37.5	0.5	15	20/50
(c2)	CMLE	8	1/8	37.5	0.5	15	20/50

Three scenarios are then considered: scenario (a) presents the simple case where signals are clearly parted. Scenarios (b) and (c) present the case when the secondary signal is within 1 chip, and therefore there exists a strong interference between both signals. For illustrative purposes we show the normalized cross-correlation function (CCF) in these three scenarios for both signals in Figure 2.

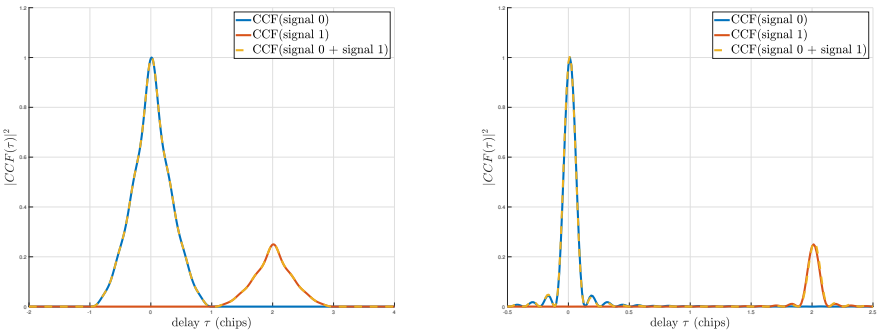

Figure 2. *Cont.*

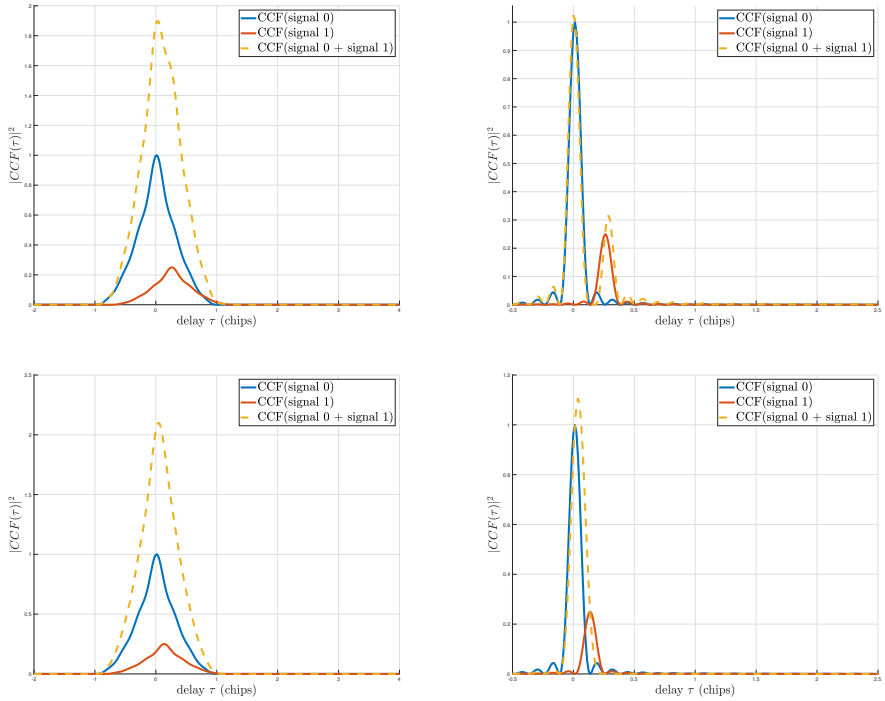

Figure 2. Normalized Cross-Correlation Function (CCF) for a GPS L1 C/A signal (**left**) and a chirp signal (**right**) for scenario (a) (top, $\Delta\tau = 2$ chips), scenario (b) (middle, $\Delta\tau = 1/4$ chips) and scenario (c) (bottom, $\Delta\tau = 1/8$ chips). In these figures, the LOS and NLOS signals are in phase ($\Delta\phi = 0^\circ$) and the amplitude of the secondary signal is half the amplitude of the main one ($\rho_1 = \rho_0/2$).

5.2. Results

5.2.1. Scenario (a): $\Delta\tau$ Larger than 1 Chip

In this scenario, we consider a relative delay of two L1 C/A chips, which corresponds to a path difference around 600 m. In this case, the two signals are clearly parted (see Figure 2 (top)) and the estimation of the main signal could almost be decoupled from the estimation of the secondary signal. Figure 3 (left hand side plots) shows the root mean square error (RMSE) for the time-delay estimation. One can see the threshold for the chirp signal at SNR_OUT = 20 dB (i.e., the SNR at the output of the matched filter) and for the GPS L1 C/A signal at SNR_OUT = 21 dB. For a SNR_OUT larger than this threshold the estimator reaches the CRB: (1) this validates the new CRB expression, and (2) provides the receiver conditions to be in a correct operation region. It is worth pointing out the impact that having two sources have on the time-delay estimation w.r.t. the single source case, where the threshold region for a GPS signal is at SNR_OUT = 15 dB (refer to [17,18]). Figure 3 (right hand side plots) show the RMSE for the Doppler frequency estimation. In this case, the performance for both direct and reflected signals is on the CRB in the range of SNR_OUT values considered. Notice that it does not make sense to consider lower SNR values because in such case the time-delay estimate is below the convergence threshold. In any case, this result validates again the CRB expression.

5.2.2. Scenario (b): $\Delta\tau$ Smaller Than 1 chip

In this scenario, we consider a relative delay of a quarter of a chip, which is about 75 m in path difference. In this case, there is a strong interference between the two signals (see Figure 2 (middle)). The results are shown in Figure 4 where again top plots are for the GPS L1 C/A signal, bottom plots for the chirp, left plots for the time-delay estimation and right plots for the Doppler frequency estimation. In this case we observe that even with such a strong interference, the time-delay estimation with a sub-optimal CRE is possible. We can notice that having a close secondary signal has an impact on the

estimation threshold, which is now SNR_OUT = 22 dB for the chirp signal, and SNR_OUT = 27 dB for the GPS signal. As expected the impact is larger for the GPS signal because of its correlation function, as it is shown in Figure 2 (middle-left). This impact can also be acknowledged in the Doppler frequency estimation, where for the GPS signal threshold region appears.

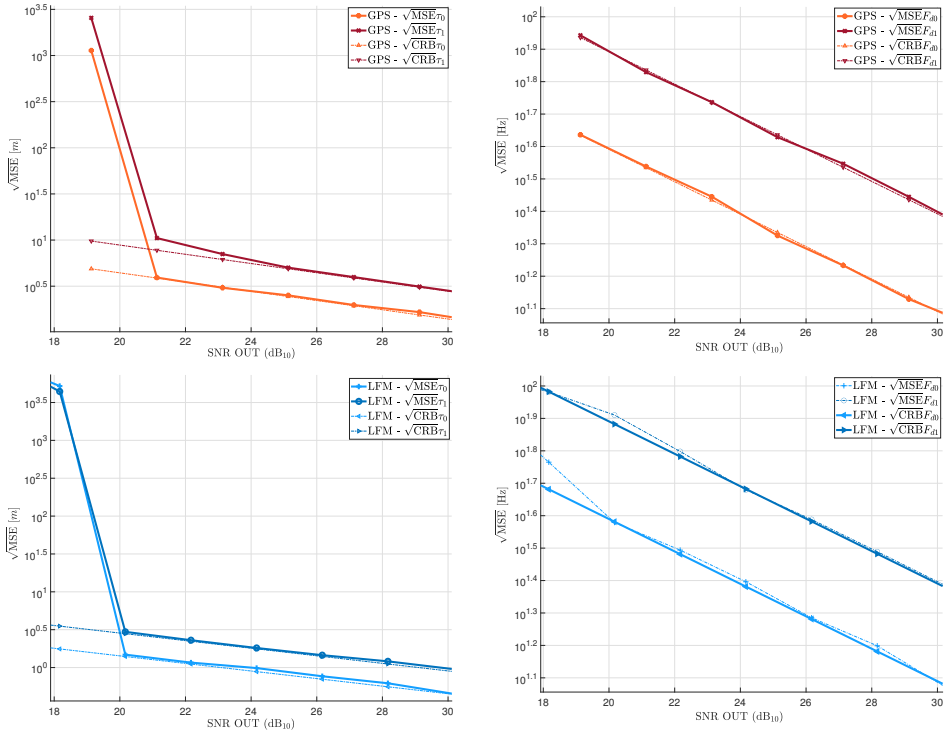

Figure 3. Scenario (a): Estimation of the delay (**left**) and the Doppler frequency (**right**) for $\Delta\tau = 2$ chips with CRE. (**top**) is for a GPS L1 C/A signal, (**bottom**) is for an LFM chirp signal.

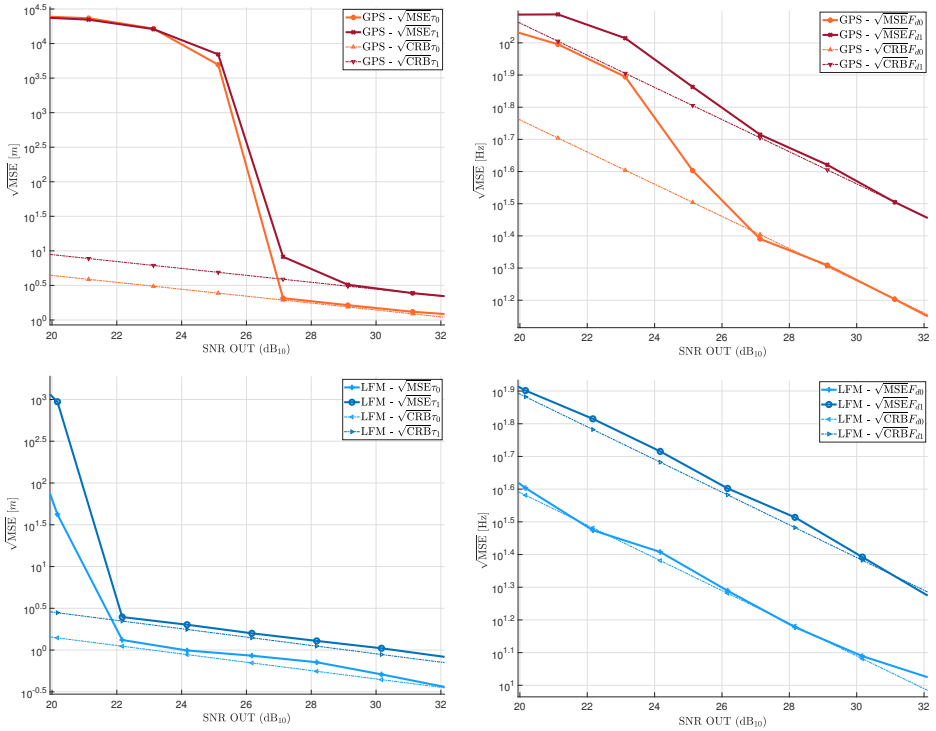

Figure 4. Scenario (b): Estimation of the delay (**left**) and the Doppler frequency (**right**) for $\Delta\tau = 1/4$ chips with CRE. (**top**) is for a GPS L1 C/A signal, (**bottom**) is for an LFM chirp signal.

5.2.3. Scenario (c): $\Delta\tau$ smaller than 1 chip

In this scenario, we consider a relative delay of an eigth of a L1 C/A chip, which accounts for a path delay of about 37.5m. In this case, there is such a strong interference between the two signals (see Figure 2 (bottom)) that the CRE cannot be efficient anymore. The CRE limit is clearly shown in Figure 5. For both signals, the time-delay estimation never reaches the optimal performances set by the CRB. Interestingly, the chirp signal seems to be more robust for the Doppler estimation, reaching the CRB for the direct signal but not for the reflected one.

Figure 6 shows the results for the dual source CMLE. One can observe a good fit between the MSE and the CRB. This result supports the fact that the CRE limitations can be overcome by the CMLE, and also validates again the CRB expression for the dual source estimation problem derived in this contribution.

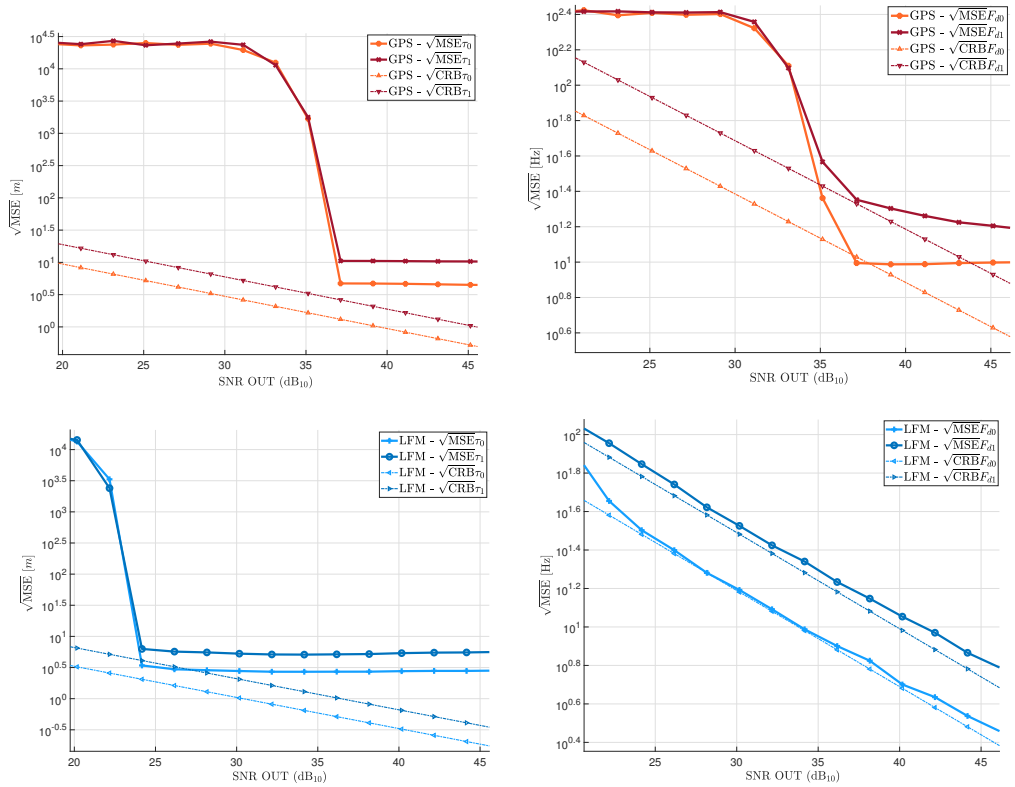

Figure 5. Scenario (c1): Estimation of the delay (**left**) and the Doppler frequency (**right**) for $\Delta\tau = 1/8$ chips with CRE. (**top**) is for a GPS L1 C/A signal, (**bottom**) is for an LFM chirp signal.

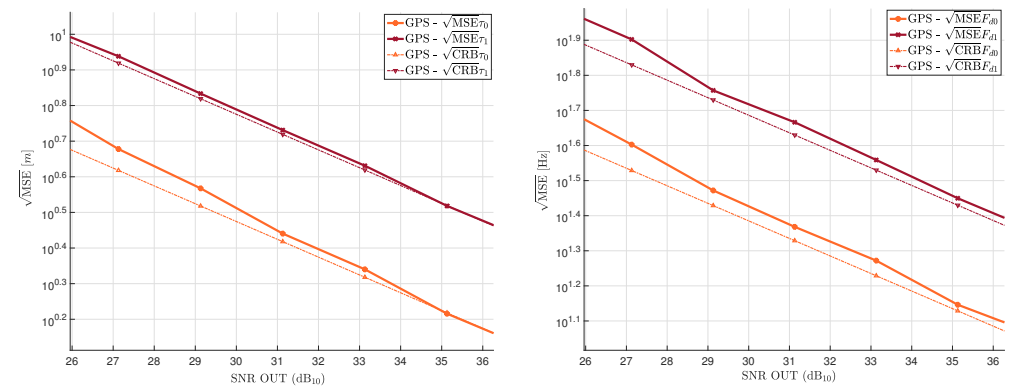

Figure 6. *Cont.*

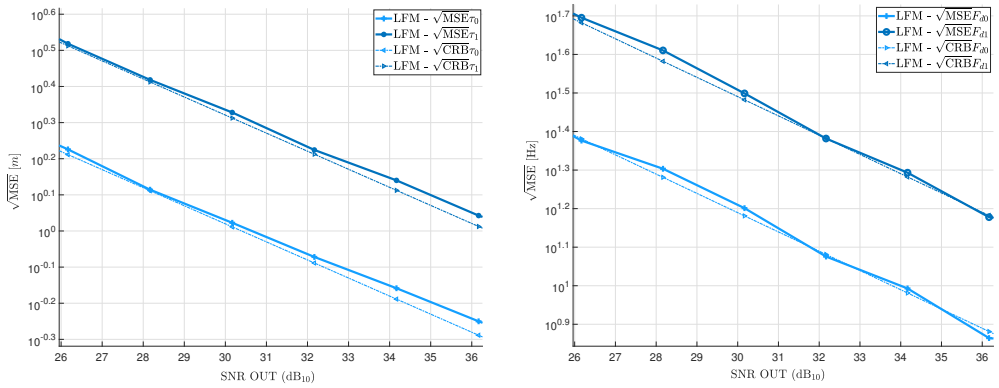

Figure 6. Scenario (c2): Estimation of the delay (**left**) and the Doppler frequency (**right**) for $\Delta\tau = 1/8$ chips with dual source CMLE. (**top**) is for a GPS L1 C/A signal, (**bottom**) is for an LFM chirp signal.

6. Further Insights and Outlooks

6.1. Comparison with Existing Literature

As previously mentioned, a formulation of the CRBs in the dual source context was proposed in [28]. In this reference, authors tackled the study of the best achievable performance in the estimation of a receiver altitude using GNSS-R. Starting from the Slepian-Bangs formula, they derived a general FIM that is similar to the one presented in Section 3. The main difference between the two formulations is that in [28], the study is done under the assumption of a static, ground-based receiver. This assumption allows the authors to set the two Doppler shifts at the same value. One can find a way to connect the results presented in Section 3 with the one proposed in [28]. Indeed, setting an equality such as $b_0 = b_1$, which constrains the current model, can be seen as a reparameterization of the vector of unknown parameters $\boldsymbol{\epsilon}$ [31]. We therefore consider the following vector transform,

$$b_0 = b_1 \Leftrightarrow \boldsymbol{\epsilon} = \boldsymbol{\epsilon}(\boldsymbol{\xi}), \tag{29}$$

where

$$\begin{aligned}\boldsymbol{\epsilon} &= \left[\begin{array}{cccccccccc} \sigma_n^2 & \tau_0 & b_0 & \rho_0 & \phi_0 & \tau_1 & b_1 & \rho_1 & \phi_1 \end{array}\right]^T,\\ \boldsymbol{\xi} &= \left[\begin{array}{cccccccccc} \sigma_n^2 & \tau_0 & b_0 & \rho_0 & \phi_0 & \tau_1 & \rho_1 & \phi_1 \end{array}\right]^T.\end{aligned}$$

From this, if we note the 9-by-9 unity matrix $\mathbf{I}_9 = [\mathbf{e}_1 \dots \mathbf{e}_9]$ with $\mathbf{e}_i$ the column unit vector with 1 at the ith component and 0 elsewhere, the relation (29) can be explicitly written as follows,

$$\boldsymbol{\epsilon}(\boldsymbol{\xi}) = \left[\begin{array}{cccccccc} \mathbf{e}_1 & \mathbf{e}_2 & \mathbf{e}_3 + \mathbf{e}_7 & \mathbf{e}_4 & \mathbf{e}_5 & \mathbf{e}_6 & \mathbf{e}_8 & \mathbf{e}_9 \end{array}\right] \boldsymbol{\xi} = \frac{\partial \boldsymbol{\epsilon}(\boldsymbol{\xi})}{\partial \boldsymbol{\xi}^T} \boldsymbol{\xi}. \tag{30}$$

Now if we consider a reparameterization of the pdf $p(\mathbf{x}; \boldsymbol{\epsilon})$ for the unknown parameters $\boldsymbol{\epsilon}$ where

$$\boldsymbol{\epsilon} = \boldsymbol{\epsilon}(\boldsymbol{\xi}), \quad \dim\{\boldsymbol{\xi}\} = 8, \quad \dim\{\boldsymbol{\epsilon}\} = 9,$$

then $p(\mathbf{x}; \boldsymbol{\xi}) = p(\mathbf{x}; \boldsymbol{\epsilon}(\boldsymbol{\xi}))$ and by use of the derivation chain rule identity,

$$\frac{\partial \ln p(\mathbf{x}; \boldsymbol{\xi})}{\partial \boldsymbol{\xi}^T} = \frac{\partial \ln p(\mathbf{x}; \boldsymbol{\epsilon}(\boldsymbol{\xi}))}{\partial \boldsymbol{\epsilon}^T} \frac{\partial \boldsymbol{\epsilon}(\boldsymbol{\xi})}{\partial \boldsymbol{\xi}^T} \Leftrightarrow \frac{\partial \ln p(\mathbf{x}; \boldsymbol{\xi})}{\partial \boldsymbol{\xi}} = \left(\frac{\partial \boldsymbol{\epsilon}(\boldsymbol{\xi})}{\partial \boldsymbol{\xi}^T}\right)^T \frac{\partial \ln p(\mathbf{x}; \boldsymbol{\epsilon}(\boldsymbol{\xi}))}{\partial \boldsymbol{\epsilon}},$$

we easily obtain that [46]

$$\mathbf{F}_{\xi|\xi}(\boldsymbol{\xi}) = E\left\{\frac{\partial \ln p(\mathbf{x}; \boldsymbol{\xi})}{\partial \boldsymbol{\xi}} \left(\frac{\partial \ln p(\mathbf{x}; \boldsymbol{\xi})}{\partial \boldsymbol{\xi}}\right)^T\right\} = \left(\frac{\partial \boldsymbol{\epsilon}(\boldsymbol{\xi})}{\partial \boldsymbol{\xi}^T}\right)^T \mathbf{F}_{\epsilon|\epsilon}\left(\boldsymbol{\epsilon}(\boldsymbol{\xi})\right) \frac{\partial \boldsymbol{\epsilon}(\boldsymbol{\xi})}{\partial \boldsymbol{\xi}^T}. \tag{31}$$

Developing the right-hand side of (31), one can obtain the following FIM (refer to Appendix B for more details on the different matrices),

$$\mathbf{F}_{\boldsymbol{\xi}|\boldsymbol{\xi}}(\boldsymbol{\xi}) = \begin{bmatrix} F_{\sigma_n^2|\boldsymbol{\xi}}(\boldsymbol{\xi}) & \mathbf{0} & \mathbf{0} \\ \mathbf{0} & \mathbf{F}_{\theta_0|\boldsymbol{\xi}}(\boldsymbol{\xi}) & \mathbf{F}_{\theta_0,\tau_1,\rho_1,\phi_1|\boldsymbol{\xi}}(\boldsymbol{\xi}) \\ \mathbf{0} & \mathbf{F}_{\tau_1,\rho_1,\phi_1,\theta_0|\boldsymbol{\xi}}(\boldsymbol{\xi}) & \mathbf{F}_{\tau_1,\rho_1,\phi_1|\boldsymbol{\xi}}(\boldsymbol{\xi}) \end{bmatrix}. \tag{32}$$

It appears that from the CRB presented in this contribution, it is possible to deduce the specific scenario studied in [28]. However, in other scenarios, the Doppler shifts of the LOS and the NLOS signals may be different (e.g., if the signal is reflected from a moving object [47]) and a more general approach is needed, for which the result in [28] is not valid and the proposed CRB provides an answer.

Another key difference between the two contributions is that the results in the present contribution are expressed directly using the baseband signal samples, whereas in [28] they are expressed with the signal Power Spectral Density (PSD). Therefore, w.r.t. [28], the calculations in this article went a little further: exploiting the Fourier transform properties over the hermitian product it is possible to jump from the PSD back to the baseband signal samples, as it is done in Appendix A and in [16]. From this remark, it is possible to express the CRB for the estimation of the altitude h of a receiver with the baseband signal samples, in the case where the signal is real and the path difference is large enough, so that the interference terms can be neglected,

$$\mathrm{CRB}_{h|\boldsymbol{\epsilon}} = \frac{\sigma_n^2 c^2 \left(1 + (\rho_1/\rho_0)^2\right)}{8\rho_1^2 \sin^2(e) F_s W_{3,3}} \tag{33}$$

where c is the speed of light in vacuum and e is the elevation angle of the transmitter seen from the specular point (see Figure 1). $W_{3,3}$ expression is recalled in (12). Note that this expression covers a broader area since it was obtained without any assumption on the Doppler shifts.

6.2. Possible CRB Applications

The CRB formulation proposed in this contribution being easy to manipulate (i.e., as it is expressed in terms of the baseband signal samples), several use cases can be identified. Hereafter is a non-exhaustive list of examples that could lead to further studies, to support the discussion and show that the proposed CRBs are of broad interest.

- As a direct extension of the results presented in the previous Section 6.1, one could look for the different parameters that can be obtained from $\boldsymbol{\epsilon}$, and calculate a new CRB dedicated to these specific parameters. In [28], the study applied to the GNSS-R altimetry problem, investigates the receiver altitude and the complex ratio between the reflected and the direct amplitudes. A generalization of this method can easily be outlined as follows. The first step is to translate either the constraints or the new variables into a transform similarly to (29), then the general expression (31) yields the corresponding FIM. If it is simple enough, a matrix inversion might end up to a closed-form expression of the CRB.
- Another application could be the assessment of the impact the secondary signal has on the main signal's parameters estimation. From the CRB expression it is indeed quite simple to extract the CRB for the time-delay estimation while there is no reflection, and the same CRB when the NLOS signals interfere with the LOS one. Such study may bring a new tool to characterize the signal robustness to multipath, being a key issue for instance in safety-critical GNSS applications, an ultimately drive the future generation of signal design.
- Again in the GNSS context, such CRBs can also be used to have an optimal performance assessment of the Carrier-to-Noise Density Ratio (C/N_0) estimation under multipath conditions. Notice that the C/N_0 is an important parameter used in several GNSS applications.

- Regarding precise positioning techniques such as real time kinematics (RTK), needed in modern applications, these CRBs may bring a valuable information on the impact that multipath may have on the final position estimate. Indeed, it is known that RTK solutions are not able to fix the carrier phase ambiguities under harsh propagation conditions such as strong multipath. This would extend the results presented in [17,18,35] to more realistic conditions.
- In the dual antenna GNSS-R context, the dual source CRB proposed in this contribution can be exploited in order to characterize the impact that an imperfect isolation between antennas may have on the final GNSS-R product. This may account for the reflected signal leaking into the upward antenna, or the LOS signal contaminating the downward one.
- Finally, a compact CRB expression can be exploited to do optimal signal design as suggested in [16]. As an example, we can study the case of the estimation of the receiver altitude (33). It was shown that the optimal signal can be linked to the first eigenvector of the matrix $\mathbf{V}^{\Delta,2}(0)$. The optimal CRB would then be given by:

$$\mathrm{CRB}_{h|\epsilon} \geq \mathrm{CRB}_{h|\epsilon}^{\mathrm{opt.}} = \frac{\sigma_n^2 c^2 \left(1 + (\rho_1/\rho_0)^2\right)}{8\rho_1^2 \sin^2(e) F_s w_1 D_{1,1}}, \tag{34}$$

  where $\pi \leq D_{1,1} \leq \pi^2$ is the largest eigenvalue of $\mathbf{V}^{\Delta,2}(0)$.

7. Conclusions

In this contribution, a new compact CRB for the joint delay, Doppler and complex amplitude estimation of a dual source narrowband CSM was derived. A handy closed-form expression of these CRBs that only depends on the baseband signal samples was also proposed. Such formulation is especially easy to use whatever the baseband signal considered, therefore being valid for a large variety of applications and of broad interest. The new formulation was validated using the asymptotic properties of the dual source CMLE and a sub-optimal algorithm, the CRE, that behaves well under certain assumptions. The different simulations show a satisfying fit between the theoretical bounds and the statistical output of the estimators applied to two representative navigation and radar signals, which validated the proposed CRBs. In addition, a brief comparison with the existing literature was provided, showing the consistency with CRBs previously derived for GNSS-R applications. A number of applications can be thought of based on these CRBs, which were also discussed for completeness. For instance, the new CRBs can be exploited for optimal signal design, multipath characterization, precise positioning methods assessment under challenging propagation conditions, or for the estimation of specific application-dependent parameters that are function of the signals parameters (delay, Doppler shift, complex amplitude).

Author Contributions: Conceptualization, E.C.; Formal analysis, C.L.; Funding acquisition, J.V.-V., L.L. and E.C.; Methodology, E.C.; Software, C.L. and L.O.; Supervision, J.V.-V. and E.C.; Validation, C.L., L.O., J.V.-V. and E.C.; Writing—original draft, C.L.; Writing—review & editing, L.O., J.V.-V. and E.C. All authors have read and agreed to the published version of the manuscript.

Funding: This research was partially supported by the CNES and the DGA/AID projects (2019.65.0068.00.470.75.01, 2018.60.0072.00.470.75.01).

Conflicts of Interest: The authors declare no conflict of interest.

Abbreviations

The following abbreviations are used in this manuscript:

CCF	Cross-Correlation Function
CMLE	Conditional Maximul Likelihood Estimator
CRB	Cramér Rao Bound
CRE	CLEAN RELAX Estimator
CSM	Conditional Signal Model

FIM	Fisher Information Matrix
GNSS	Global Navigation Satellite System
GNSS-R	GNSS Reflectometry
GPS	Global Positioning System
LFM	Linear Frequency Modulated
LOS	Line-Of-Sight
MEDLL	Multipath Mitigating Delay Lock Loop
MMT	Multipath Mitigation Technique
MSE	Mean Square Error
MVU	Minumum Variance Unbiased
NLOS	Non-Line-Of-Sight
pdf	Probability Density Function
PSD	Power Spectral Density
RMSE	Root Mean Square Error
RTK	Real Time Kinematics
SNR	Signal-to-Noise Ratio

Appendix A. Details of the Derivation of the Fisher Information Matrix

Appendix A.1. Prior Calculation on Fourier Transforms

In order to compute the FIM we need to know the Fourier transform of a set of functions. First, remembering that the signal is band-limited of band $B \leq F_s$, we have,

$$s(t) \rightleftharpoons S(f) = \left(\frac{1}{F_s} \sum_{n=N_1}^{N_2} s(nT_s) e^{-j2\pi f n T_s} \right) 1_{\left[-\frac{F_s}{2};\frac{F_s}{2}\right]}. \tag{A1}$$

In order to tackle the issue that may come from the spectral shift due to the Doppler effect, we simply need to take F_s large enough so that $\frac{F_s}{2} \geq \frac{B}{2} + f_c \max\{|b_0|, |b_1|, |\Delta b|\}$ ($\Delta b = b_1 - b_0$),

$$s(t)e^{j2\pi f_c b t} \rightleftharpoons S(f - f_c b) = \left(\frac{1}{F_s} \sum_{n=N_1}^{N_2} s(nT_s) e^{-j2\pi (f - f_c b) n T_s} \right) 1_{\left[-\frac{F_s}{2};\frac{F_s}{2}\right]}. \tag{A2}$$

Let s_0 be defined by $s_0(t;\tau) = s(t-\tau)$, then we have that,

$$(t-\tau)s_0(t;\tau) = t s_0(t;\tau) - \tau s_0(t;\tau), \tag{A3}$$

and

$$\begin{aligned} (t-\tau)s(t-\tau) &\rightleftharpoons \frac{j}{2\pi}\frac{\mathrm{d}}{\mathrm{d}f}\left(S(f)e^{-j2\pi f\tau}\right) - \tau S(f)e^{-j2\pi f\tau} \\ &\rightleftharpoons \frac{j}{2\pi}\frac{\mathrm{d}}{\mathrm{d}f}(S(f))e^{-j2\pi f\tau}. \end{aligned} \tag{A4}$$

Now let s_1 be defined by $s_1(t;b) = s(t)e^{j2\pi f_c b t}$. We have the known result that,

$$t s_1(t;b) \rightleftharpoons \frac{j}{2\pi}\frac{\mathrm{d}}{\mathrm{d}f}\left(s_1(t;b)\right),$$

and therefore,

$$t s(t) e^{j2\pi f_c b t} \rightleftharpoons \frac{j}{2\pi}\frac{\mathrm{d}}{\mathrm{d}f}\left(S(f - f_c b)\right). \tag{A5}$$

On the other hand,

$$s_1^{(1)}(t;b) = s^{(1)}(t)e^{j2\pi f_c bt} + j2\pi f_c b s_1(t;b)$$
$$\Leftrightarrow\ s^{(1)}(t)e^{j2\pi f_c bt} = s_1^{(1)}(t;b) - j2\pi f_c b s_1(t;b),$$

then, we directly have that,

$$s^{(1)}(t)e^{j2\pi f_c bt} \rightleftharpoons j2\pi\,(f - f_c b)\,S(f - f_c b). \tag{A6}$$

Finally if we now define s_2 as $s_2(t;b) = ts(t)e^{j2\pi f_c bt}$,

$$s_2^{(1)}(t;b) = s_1(t;b) + ts^{(1)}(t)e^{j2\pi f_c bt} + (j2\pi f_c b)s_2(t;b)$$
$$\Leftrightarrow\ ts^{(1)}(t)e^{j2\pi f_c bt} = -s_1(t;b) + s_2^{(1)}(t;b) - (j2\pi f_c b)s_2(t;b),$$

therefore,

$$ts^{(1)}(t)e^{j2\pi f_c bt} \rightleftharpoons -S(f - f_c b) + j2\pi(f - f_c b)\frac{\mathrm{d}}{\mathrm{d}f}\left(S(f - f_c b)\right). \tag{A7}$$

Appendix A.2. Bounds Derivation

Hereafter we provide details on the derivation of the FIM (9). Given the signal model (3), the derivative of the parameters vector excluding the noise variance σ_n^2, $\bar{\boldsymbol{\epsilon}}$, can be expressed in a matrix form as

$$\frac{\partial}{\partial \bar{\boldsymbol{\epsilon}}}\left(\boldsymbol{d}(t;\boldsymbol{\theta}_0) + \boldsymbol{d}(t;\boldsymbol{\theta}_1)\right) = \mathbf{Q}(\bar{\boldsymbol{\epsilon}})\mathcal{D}(t;\bar{\boldsymbol{\epsilon}})\mathbf{e}(t;\bar{\boldsymbol{\epsilon}}), \tag{A8}$$

where

$$\mathbf{Q}(\bar{\boldsymbol{\epsilon}}) = \begin{bmatrix} \mathbf{Q}_0 & \mathbf{0} \\ \mathbf{0} & \mathbf{Q}_1 \end{bmatrix},\ \mathbf{Q}_i = \begin{bmatrix} j\rho_i w_c b_i & 0 & -\rho_i \\ 0 & -j\rho_i w_c & 0 \\ 1 & 0 & 0 \\ j\rho_i & 0 & 0 \end{bmatrix}, \tag{A9}$$

$$\mathcal{D}(t;\bar{\boldsymbol{\epsilon}}) = \begin{bmatrix} s(t-\tau_0) & 0 \\ (t-\tau_0)s(t-\tau_0) & 0 \\ s^{(1)}(t-\tau_0) & 0 \\ 0 & s(t-\tau_1) \\ 0 & (t-\tau_1)s(t-\tau_1) \\ 0 & s^{(1)}(t-\tau_1) \end{bmatrix}, \tag{A10}$$

$$\mathbf{e}(t;\bar{\boldsymbol{\epsilon}}) = \begin{pmatrix} e^{j\psi_0}e^{-j\omega_c b_0 t} \\ e^{j\psi_1}e^{-j\omega_c b_1 t} \end{pmatrix},\ \text{with } \psi_i = \phi_i + \omega_c b_i \tau_i \tag{A11}$$

Therefore, the derivative of the vector $\mathbf{A}\boldsymbol{\alpha}$ (when $t = nT_s$) w.r.t $\bar{\boldsymbol{\epsilon}}$ is

$$\left(\frac{\partial \mathbf{A}\boldsymbol{\alpha}}{\partial \bar{\boldsymbol{\epsilon}}}\right)^T = \mathbf{Q}(\bar{\boldsymbol{\epsilon}})\left[\ldots,\ \mathcal{D}(nT_s;\bar{\boldsymbol{\epsilon}})\mathbf{e}(nT_s;\bar{\boldsymbol{\epsilon}}),\ \ldots\right]_{N_1 \le n \le N_2}. \tag{A12}$$

From this result we can write that

$$\left(\frac{\partial \mathbf{A}\boldsymbol{\alpha}}{\partial \bar{\boldsymbol{\epsilon}}^T}\right)^H \left(\frac{\partial \mathbf{A}\boldsymbol{\alpha}}{\partial \bar{\boldsymbol{\epsilon}}^T}\right) =$$
$$\mathbf{Q}(\bar{\boldsymbol{\epsilon}})^* \left(\sum_{n=N_1}^{N_2} \mathcal{D}(nT_s;\bar{\boldsymbol{\epsilon}})^* \left(\mathbf{I}_2 + \boldsymbol{\Delta}_{\boldsymbol{\theta}}(nT_s;\bar{\boldsymbol{\epsilon}})^*\right)\mathcal{D}(nT_s;\bar{\boldsymbol{\epsilon}})^T\right)\mathbf{Q}(\bar{\boldsymbol{\epsilon}})^T, \tag{A13}$$

with $\boldsymbol{\Delta}_{\boldsymbol{\theta}}$ induced by the difference of delay, Doppler shifts and phase between the two signals,

$$\begin{aligned}\boldsymbol{\Delta}_{\boldsymbol{\theta}}(nT_s;\bar{\boldsymbol{\epsilon}}) &\triangleq \mathbf{e}(nT_s;\bar{\boldsymbol{\epsilon}})\mathbf{e}(nT_s;\bar{\boldsymbol{\epsilon}})^H - \mathbf{I}_2 \\ &= \begin{bmatrix} 0 & e^{-j\Delta\psi}e^{j2\pi f_c \Delta b n T_s} \\ e^{j\Delta\psi}e^{-j2\pi f_c \Delta b n T_s} & 0 \end{bmatrix},\end{aligned} \tag{A14}$$

with

$$\Delta\psi = \psi_1 - \psi_0 = \Delta\phi + \omega_c(b_1\tau_1 - b_0\tau_0),\ \Delta b = b_1 - b_0,\ \Delta\phi = \phi_1 - \phi_0. \tag{A15}$$

Similarly to [16], taking the limit of (A13) when N_1' and N_2' are very large leads to an integral form

$$\begin{aligned}&\lim_{(N_1,N_2)\to(-\infty,+\infty)} \left(\frac{\partial \mathbf{A}\boldsymbol{\alpha}}{\partial \bar{\boldsymbol{\epsilon}}^T}\right)^H \left(\frac{\partial \mathbf{A}\boldsymbol{\alpha}}{\partial \bar{\boldsymbol{\epsilon}}^T}\right) \\ &\qquad = F_s \left(\mathbf{Q}(\bar{\boldsymbol{\epsilon}}) \begin{bmatrix} \mathbf{W}_0 & (\mathbf{W}^{\Delta})^H \\ \mathbf{W}^{\Delta} & \mathbf{W}_1 \end{bmatrix} \mathbf{Q}(\bar{\boldsymbol{\epsilon}})^H\right)^*,\end{aligned} \tag{A16}$$

where $\mathbf{W}_0$ and $\mathbf{W}_1$ are derived and studied in the single source case in [17,18] and

$$\mathbf{W}^{\Delta} \triangleq \begin{bmatrix} W_{1,1}^{\Delta} & W_{1,2}^{\Delta} & W_{1,3}^{\Delta} \\ W_{2,1}^{\Delta} & W_{2,2}^{\Delta} & W_{2,3}^{\Delta} \\ W_{3,1}^{\Delta} & W_{3,2}^{\Delta} & W_{3,3}^{\Delta} \end{bmatrix} e^{j\Delta\psi}e^{-j\omega_c\Delta b\tau_0}, \tag{A17}$$

with

$$W_{1,1}^{\Delta} = e^{j\omega_c\Delta b\tau_0}\int_{\mathbb{R}} s(t-\tau_1)s(t-\tau_0)^* e^{-j\omega_c\Delta bt}\mathrm{d}t, \tag{A18}$$

$$W_{1,2}^{\Delta} = e^{j\omega_c\Delta b\tau_0}\int_{\mathbb{R}} (t-\tau_0)s(t-\tau_1)s(t-\tau_0)^* e^{-j\omega_c\Delta bt}\mathrm{d}t, \tag{A19}$$

$$W_{1,3}^{\Delta} = e^{j\omega_c\Delta b\tau_0}\int_{\mathbb{R}} s(t-\tau_1)s^{(1)}(t-\tau_0)^* e^{-j\omega_c\Delta bt}\mathrm{d}t, \tag{A20}$$

$$W_{2,1}^{\Delta} = e^{j\omega_c\Delta b\tau_0}\int_{\mathbb{R}} (t-\tau_1)s(t-\tau_1)s(t-\tau_0)^* e^{-j\omega_c\Delta bt}\mathrm{d}t, \tag{A21}$$

$$W_{2,2}^{\Delta} = e^{j\omega_c\Delta b\tau_0}\int_{\mathbb{R}} (t-\tau_1)(t-\tau_0)s(t-\tau_1)s(t-\tau_0)^* e^{-j\omega_c\Delta bt}\mathrm{d}t, \tag{A22}$$

$$W_{2,3}^{\Delta} = e^{j\omega_c\Delta b\tau_0}\int_{\mathbb{R}} (t-\tau_1)s(t-\tau_1)s^{(1)}(t-\tau_0)^* e^{-j\omega_c\Delta bt}\mathrm{d}t, \tag{A23}$$

$$W_{3,1}^{\Delta} = e^{j\omega_c\Delta b\tau_0}\int_{\mathbb{R}} s^{(1)}(t-\tau_1)s(t-\tau_0)^* e^{-j\omega_c\Delta bt}\mathrm{d}t, \tag{A24}$$

$$W_{3,2}^{\Delta} = e^{j\omega_c\Delta b\tau_0}\int_{\mathbb{R}} (t-\tau_0)s^{(1)}(t-\tau_1)s(t-\tau_0)^* e^{-j\omega_c\Delta bt}\mathrm{d}t, \tag{A25}$$

$$W_{3,3}^{\Delta} = e^{j\omega_c\Delta b\tau_0}\int_{\mathbb{R}} s^{(1)}(t-\tau_1)s^{(1)}(t-\tau_0)^* e^{-j\omega_c\Delta bt}\mathrm{d}t. \tag{A26}$$

Exploiting the Fourier transform properties over the hermitian product and the relations recalled in Appendix A.1, one can work these integral expressions as follows:

$$W_{1,1}^{\Delta} = e^{j\omega_c\Delta b\tau_0}\int_{\mathbb{R}} s(t-\tau_1)s(t-\tau_0)^* e^{-j2\pi f_c\Delta bt}\mathrm{d}t = s(u-\Delta\tau)s(u)^* e^{-j2\pi f_c\Delta bu}\mathrm{d}u,$$

$$W_{1,1}^{\Delta} = \int_{\mathbb{R}} s(u-\Delta\tau)\underbrace{\left(s(u)e^{j2\pi f_c\Delta bu}\right)^*}_{\text{(A2)}}\mathrm{d}u = \int_{-\frac{F_s}{2}}^{\frac{F_s}{2}} S(f)e^{-j2\pi f\Delta\tau}S(f-f_c\Delta b)^*\mathrm{d}f,$$

and using the sum definition of the Fourier transform (A1),

$$W_{1,1}^{\Delta} = \frac{1}{F_s}\int_{-\frac{1}{2}}^{\frac{1}{2}} \left(\mathbf{s}^T\boldsymbol{\nu}(f)^*\right)e^{-j2\pi f\frac{\Delta\tau}{T_s}}\left(\mathbf{s}^H\mathbf{U}\boldsymbol{\nu}(f)\right)\mathrm{d}f = \frac{1}{F_s}\mathbf{s}^H\mathbf{U}\left(\Delta b\right)\mathbf{V}^{\Delta,0}\left(\frac{\Delta\tau}{T_s}\right)\mathbf{s}. \tag{A27}$$

Following the same procedure we have that,

$$
\begin{aligned}
W_{1,2}^{\Delta} &= e^{j\omega_c \Delta b \tau_0} \int_{\mathbb{R}} (t-\tau_0) s(t-\tau_1) s(t-\tau_0)^* e^{-j2\pi f_c \Delta b t} \mathrm{d}t = \int_{\mathbb{R}} u s(u-\Delta\tau) s(u)^* e^{-j2\pi f_c \Delta b u} \mathrm{d}u, \\
W_{1,2}^{\Delta} &= \int_{\mathbb{R}} s(u-\Delta\tau) \underbrace{\left(u s(u) e^{j2\pi f_c \Delta b u} \right)^*}_{\text{(A5)}} \mathrm{d}u = \int_{-\frac{F_s}{2}}^{\frac{F_s}{2}} S(f) e^{-j2\pi f \Delta\tau} \left(\frac{j}{2\pi} \frac{\mathrm{d}}{\mathrm{d}f} \left(S(f - f_c \Delta b) \right) \right)^* \mathrm{d}f \\
&= \frac{1}{F_s^2} \int_{-\frac{1}{2}}^{\frac{1}{2}} \left(\mathbf{s}^T \boldsymbol{\nu}(f)^* \right) e^{-j2\pi f \frac{\Delta\tau}{T_s}} \left(\mathbf{s}^H \mathbf{D}\mathbf{U}(\Delta b) \boldsymbol{\nu}(f) \right) \mathrm{d}f \\
&= \frac{1}{F_s^2} \mathbf{s}^H \mathbf{D}\mathbf{U}(\Delta b) \mathbf{V}^{\Delta,0} \left(\frac{\Delta\tau}{T_s} \right) \mathbf{s}, \qquad \text{(A28)}
\end{aligned}
$$

$$
\begin{aligned}
W_{1,3}^{\Delta} &= e^{j\omega_c \Delta b \tau_0} \int_{\mathbb{R}} s(t-\tau_1) s^{(1)}(t-\tau_0)^* e^{-j2\pi f_c \Delta b t} \mathrm{d}t = \int_{\mathbb{R}} s(u-\Delta\tau) s^{(1)}(u)^* e^{-j2\pi f_c \Delta b u} \mathrm{d}u, \\
W_{1,3}^{\Delta} &= \int_{\mathbb{R}} s(u-\Delta\tau) \underbrace{\left(s^{(1)}(u) e^{j2\pi f_c \Delta b u} \right)^*}_{\text{(A6)}} \mathrm{d}u \\
&= \int_{-\frac{F_s}{2}}^{\frac{F_s}{2}} \left(S(f) e^{-j2\pi f \Delta\tau} \right) \left(j2\pi (f - f_c \Delta b) S(f - f_c \Delta b) \right)^* \mathrm{d}f \\
&= \frac{1}{F_s} \int_{-\frac{1}{2}}^{\frac{1}{2}} \left(\mathbf{s}^T \boldsymbol{\nu}(f)^* \right) e^{-j2\pi f \frac{\Delta\tau}{T_s}} \left(-j2\pi F_s f \mathbf{s}^H \mathbf{U}(\Delta b) \boldsymbol{\nu}(f) + j2\pi f_c \Delta b \mathbf{s}^H \mathbf{U}(\Delta b) \boldsymbol{\nu}(f) \right) \mathrm{d}f \\
&= -\mathbf{s}^H \mathbf{U}(\Delta b) \mathbf{V}^{\Delta,1} \left(\frac{\Delta\tau}{T_s} \right) \mathbf{s} + \frac{j\omega_c \Delta b}{F_s} \mathbf{s}^H \mathbf{U}(\Delta b) \mathbf{V}^{\Delta,0} \left(\frac{\Delta\tau}{T_s} \right) \mathbf{s}, \qquad \text{(A29)} \\
W_{2,1}^{\Delta} &= e^{j\omega_c \Delta b \tau_0} \int_{\mathbb{R}} (t-\tau_1) s(t-\tau_1) s(t-\tau_0)^* e^{-j2\pi f_c \Delta b t} \mathrm{d}t \\
&= \int_{\mathbb{R}} (u-\Delta\tau) s(u-\Delta\tau) s(u)^* e^{-j2\pi f_c \Delta b u} \mathrm{d}u \\
&= \int_{\mathbb{R}} \underbrace{(u-\Delta\tau) s(u-\Delta\tau)}_{\text{(A4)}} \underbrace{\left(s(u) e^{j2\pi f_c \Delta b u} \right)^*}_{\text{(A2)}} \mathrm{d}u \\
&= \int_{-\frac{F_s}{2}}^{\frac{F_s}{2}} \left(\frac{j}{2\pi} \frac{\mathrm{d}}{\mathrm{d}f} \left(S(f) \right) e^{-j2\pi f \Delta\tau} \right) S(f - f_c \Delta b)^* \mathrm{d}f \\
&= \frac{1}{F_s^2} \int_{-\frac{1}{2}}^{\frac{1}{2}} \left(\mathbf{s}^T \mathbf{D}\boldsymbol{\nu}(f)^* \right) e^{-j2\pi f \frac{\Delta\tau}{T_s}} \left(\mathbf{s}^H \mathbf{U}(\Delta b) \boldsymbol{\nu}(f) \right) \mathrm{d}f \\
&= \frac{1}{F_s^2} \mathbf{s}^H \mathbf{U}(\Delta b) \mathbf{V}^{\Delta,0} \left(\frac{\Delta\tau}{T_s} \right) \mathbf{D}\mathbf{s}, \qquad \text{(A30)} \\
W_{2,2}^{\Delta} &= e^{j\omega_c \Delta b \tau_0} \int_{\mathbb{R}} (t-\tau_1)(t-\tau_0) s(t-\tau_1) s(t-\tau_0)^* e^{-j2\pi f_c \Delta b t} \mathrm{d}t \\
&= \int_{\mathbb{R}} u(u-\Delta\tau) s(u-\Delta\tau) s(u)^* e^{-j2\pi f_c \Delta b u} \mathrm{d}u \\
&= \int_{\mathbb{R}} \underbrace{((u-\Delta\tau) s(u-\Delta\tau))}_{\text{(A4)}} \underbrace{\left(u s(u) e^{j2\pi f_c \Delta b u} \right)^*}_{\text{(A5)}} \mathrm{d}u \\
&= \int_{-\frac{F_s}{2}}^{\frac{F_s}{2}} \left(\frac{j}{2\pi} \frac{\mathrm{d}}{\mathrm{d}f} \left(S(f) \right) e^{-j2\pi f \Delta\tau} \right) \left(\frac{j}{2\pi} \frac{\mathrm{d}}{\mathrm{d}f} \left(S(f - f_c \Delta b) \right) \right)^* \mathrm{d}f \\
&= \frac{1}{F_s^3} \int_{-\frac{1}{2}}^{\frac{1}{2}} \left(\mathbf{s}^T \mathbf{D}\boldsymbol{\nu}(f)^* \right) e^{-j2\pi f \frac{\Delta\tau}{T_s}} \left(\mathbf{s}^H \mathbf{D}\mathbf{U}(\Delta b) \boldsymbol{\nu}(f) \right) \mathrm{d}f \\
&= \frac{1}{F_s^3} \mathbf{s}^H \mathbf{D}\mathbf{U}(\Delta b) \mathbf{V}^{\Delta,0} \left(\frac{\Delta\tau}{T_s} \right) \mathbf{D}\mathbf{s}, \qquad \text{(A31)}
\end{aligned}
$$

$$
\begin{aligned}
W_{2,3}^{\Delta} &= e^{j\omega_c \Delta b \tau_0} \int_{\mathbb{R}} (t-\tau_1) s(t-\tau_1) s^{(1)}(t-\tau_0)^* e^{-j2\pi f_c \Delta b t} \mathrm{d}t \\
&= \int_{\mathbb{R}} (u-\Delta\tau) s(u-\Delta\tau) s^{(1)}(u)^* e^{-j2\pi f_c \Delta b u} \mathrm{d}u \\
&= \int_{\mathbb{R}} \underbrace{((u-\Delta\tau)s(u-\Delta\tau))}_{(A4)} \underbrace{\left(s^{(1)}(u) e^{j2\pi f_c \Delta b u}\right)^*}_{(A6)} \mathrm{d}u \\
&= \int_{-\frac{F_s}{2}}^{\frac{F_s}{2}} \left(\frac{j}{2\pi}\frac{\mathrm{d}}{\mathrm{d}f}\left(S(f)\right) e^{-j2\pi f \Delta\tau}\right) \left(j2\pi(f-f_c\Delta b) S(f-f_c\Delta b)\right)^* \mathrm{d}f \\
&= \frac{1}{F_s^2} \int_{-\frac{1}{2}}^{\frac{1}{2}} \left(\mathbf{s}^T \mathbf{D} \boldsymbol{\nu}(f)^*\right) e^{-j2\pi f \frac{\Delta\tau}{T_s}} \left(-j2\pi F_s f \mathbf{s}^H \mathbf{U}(\Delta b) \boldsymbol{\nu}(f) + j2\pi f_c \Delta b \mathbf{s}^H \mathbf{U}(\Delta b) \boldsymbol{\nu}(f)\right) \mathrm{d}f \\
&= -\frac{1}{F_s} \mathbf{s}^H \mathbf{U}(\Delta b) \mathbf{V}^{\Delta,1}\left(\frac{\Delta\tau}{T_s}\right) \mathbf{D}\mathbf{s} + \frac{j\omega_c \Delta b}{F_s^2} \mathbf{s}^H \mathbf{U}(\Delta b) \mathbf{V}^{\Delta,0}\left(\frac{\Delta\tau}{T_s}\right) \mathbf{D}\mathbf{s}, \qquad \text{(A32)}
\end{aligned}
$$

$$
W_{3,1}^{\Delta} = e^{j\omega_c \Delta b \tau_0} \int_{\mathbb{R}} s^{(1)}(t-\tau_1) s(t-\tau_0)^* e^{-j2\pi f_c \Delta b t} \mathrm{d}t = \int_{\mathbb{R}} s^{(1)}(u-\Delta\tau) s(u)^* e^{-j2\pi f_c \Delta b u} \mathrm{d}u,
$$

$$
\begin{aligned}
W_{3,1}^{\Delta} &= \int_{\mathbb{R}} s^{(1)}(u-\Delta\tau) \underbrace{\left(s(u) e^{j2\pi f_c \Delta b u}\right)^*}_{(A2)} \mathrm{d}u = \int_{-\frac{F_s}{2}}^{\frac{F_s}{2}} \left(j2\pi f S(f) e^{-j2\pi f \Delta\tau}\right) \left(S(f-f_c\Delta b)\right)^* \mathrm{d}f \\
&= \int_{-\frac{1}{2}}^{\frac{1}{2}} \left(j2\pi f \mathbf{s}^T \boldsymbol{\nu}(f)^*\right) e^{-j2\pi f \frac{\Delta\tau}{T_s}} \left(\mathbf{s}^H \mathbf{U}(\Delta b) \boldsymbol{\nu}(f)\right) \mathrm{d}f \\
&= \mathbf{s}^H \mathbf{U}(\Delta b) \mathbf{V}^{\Delta,1}\left(\frac{\Delta\tau}{T_s}\right) \mathbf{s}, \qquad \text{(A33)}
\end{aligned}
$$

$$
\begin{aligned}
W_{3,2}^{\Delta} &= e^{j\omega_c \Delta b \tau_0} \int_{\mathbb{R}} (t-\tau_0) s^{(1)}(t-\tau_1) s(t-\tau_0)^* e^{-j2\pi f_c \Delta b t} \mathrm{d}t \\
&= \int_{\mathbb{R}} s^{(1)}(u-\Delta\tau) s(u)^* e^{-j2\pi f_c \Delta b u} \mathrm{d}u \\
&= \int_{\mathbb{R}} s^{(1)}(u-\Delta\tau) \underbrace{\left(u s(u) e^{j2\pi f_c \Delta b u}\right)^*}_{(A5)} \mathrm{d}u \\
&= \int_{-\frac{F_s}{2}}^{\frac{F_s}{2}} \left(j2\pi f S(f) e^{-j2\pi f \Delta\tau}\right) \left(\frac{j}{2\pi}\frac{\mathrm{d}}{\mathrm{d}f}\left(S(f-f_c\Delta b)\right)\right)^* \mathrm{d}f \\
&= \frac{1}{F_s} \int_{-\frac{1}{2}}^{\frac{1}{2}} \left(j2\pi f \mathbf{s}^T \boldsymbol{\nu}(f)^*\right) e^{-j2\pi f \frac{\Delta\tau}{T_s}} \left(\mathbf{s}^H \mathbf{D}\mathbf{U}(\Delta b) \boldsymbol{\nu}(f)\right) \mathrm{d}f \\
&= \frac{1}{F_s} \mathbf{s}^H \mathbf{D}\mathbf{U}(\Delta b) \mathbf{V}^{\Delta,1}\left(\frac{\Delta\tau}{T_s}\right) \mathbf{s}, \qquad \text{(A34)}
\end{aligned}
$$

$$
\begin{aligned}
W_{3,3}^{\Delta} &= e^{j\omega_c \Delta b \tau_0} \int_{\mathbb{R}} s^{(1)}(t-\tau_1) s^{(1)}(t-\tau_0)^* e^{-j2\pi f_c \Delta b t} \mathrm{d}t = \int_{\mathbb{R}} s^{(1)}(u-\Delta\tau) s^{(1)}(u)^* e^{-j2\pi f_c \Delta b u} \mathrm{d}u, \\
W_{3,3}^{\Delta} &= \int_{\mathbb{R}} s^{(1)}(u-\Delta\tau) \underbrace{\left(s^{(1)}(u) e^{j2\pi f_c \Delta b u}\right)^*}_{(A6)} \mathrm{d}u \\
&= \int_{-\frac{F_s}{2}}^{\frac{F_s}{2}} \left(j2\pi f S(f) e^{-j2\pi f \Delta\tau}\right) \left(j2\pi(f-f_c\Delta b) S(f-f_c\Delta b)\right)^* \mathrm{d}f \\
&= \int_{-\frac{1}{2}}^{\frac{1}{2}} \left(j2\pi f \mathbf{s}^T \boldsymbol{\nu}(f)^*\right) e^{-j2\pi f \frac{\Delta\tau}{T_s}} \left(-j2\pi F_s f \mathbf{s}^H \mathbf{U}(\Delta b) \boldsymbol{\nu}(f) + j2\pi f_c \Delta b \mathbf{s}^H \mathbf{U}(\Delta b) \boldsymbol{\nu}(f)\right) \mathrm{d}f \\
&= F_s \mathbf{s}^H \mathbf{U}(\Delta b) \mathbf{V}^{\Delta,2}\left(\frac{\Delta\tau}{T_s}\right) \mathbf{s} + j\omega_c \Delta b \mathbf{s}^H \mathbf{U}(\Delta b) \mathbf{V}^{\Delta,1}\left(\frac{\Delta\tau}{T_s}\right) \mathbf{s}, \qquad \text{(A35)}
\end{aligned}
$$

where

$$\mathbf{s} = \left(\ \dots \quad s(nT_s) \quad \dots \ \right)^T_{N_1 \le n \le N_2}, \tag{A36}$$

$$\boldsymbol{\nu}(f) = \left(\ \dots \quad e^{j2\pi fn} \quad \dots \ \right)^T_{N_1 \le n \le N_2}, \tag{A37}$$

$$\mathbf{U}(\Delta b) = \mathrm{diag}\left(\ \dots \quad e^{-j\omega_c \Delta b n T_s} \quad \dots \ \right)_{N_1 \le n \le N_2}, \tag{A38}$$

$$\mathbf{D} = \left(\ \dots \quad n \quad \dots \ \right)^T_{N_1 \le n \le N_2}, \tag{A39}$$

$$\mathbf{V}^{\Delta,0}\left(\frac{\Delta\tau}{T_s}\right) = \int_{-\frac{1}{2}}^{\frac{1}{2}} \boldsymbol{\nu}(f)\boldsymbol{\nu}^H(f) e^{-j2\pi f \frac{\Delta\tau}{T_s}} \mathrm{d}f, \tag{A40}$$

$$\left[\mathbf{V}^{\Delta,0}\left(\frac{\Delta\tau}{T_s}\right)\right]_{k,l} = \mathrm{sinc}\left(k - l - \frac{\Delta\tau}{T_s}\right),$$

$$\mathbf{V}^{\Delta,1}\left(\frac{\Delta\tau}{T_s}\right) = j2\pi \int_{-\frac{1}{2}}^{\frac{1}{2}} f\boldsymbol{\nu}(f)\boldsymbol{\nu}^H(f) e^{-j2\pi f \frac{\Delta\tau}{T_s}} \mathrm{d}f, \tag{A41}$$

$$\left[\mathbf{V}^{\Delta,1}\left(\frac{\Delta\tau}{T_s}\right)\right]_{k,l} = \frac{1}{k - l - \frac{\Delta\tau}{T_s}} \left(\cos\left(\pi(k - l - \frac{\Delta\tau}{T_s})\right) - \mathrm{sinc}\left(k - l - \frac{\Delta\tau}{T_s}\right)\right),$$

$$\mathbf{V}^{\Delta,2}\left(\frac{\Delta\tau}{T_s}\right) = 4\pi^2 \int_{-\frac{1}{2}}^{\frac{1}{2}} f^2\boldsymbol{\nu}(f)\boldsymbol{\nu}^H(f) e^{-j2\pi f \frac{\Delta\tau}{T_s}} \mathrm{d}f, \tag{A42}$$

$$\left[\mathbf{V}^{\Delta,2}\left(\frac{\Delta\tau}{T_s}\right)\right]_{k,l} = \pi^2 \mathrm{sinc}\left(k - l - \frac{\Delta\tau}{T_s}\right) + 2\frac{cos\left(\pi(k - l - \frac{\Delta\tau}{T_s})\right) - \mathrm{sinc}\left(k - l - \frac{\Delta\tau}{T_s}\right)}{\left(k - l - \frac{\Delta\tau}{T_s}\right)^2}.$$

Appendix B. Details on the Constrained Fisher Information Matrix

We consider the vector of unknown parameters transform (29). The corresponding jacobian, initially defined in (30), can be written as follows,

$$\frac{\partial \boldsymbol{\epsilon}(\boldsymbol{\xi})}{\partial \boldsymbol{\xi}^T} = \begin{bmatrix} 1 & \mathbf{0} & \mathbf{0} \\ \mathbf{0} & \mathbf{I}_4 & \mathbf{0}_{4\times 3} \\ \mathbf{0} & \mathbf{E}_1 & \mathbf{E}_3 \end{bmatrix}, \ \mathbf{E}_1 = \begin{bmatrix} 0 & 0 & 0 & 0 \\ 0 & 1 & 0 & 0 \\ 0 & 0 & 0 & 0 \\ 0 & 0 & 0 & 0 \end{bmatrix}, \ \mathbf{E}_3 = \begin{bmatrix} 1 & 0 & 0 \\ 0 & 0 & 0 \\ 0 & 1 & 0 \\ 0 & 0 & 1 \end{bmatrix}. \tag{A43}$$

Using this representation, it is easy to develop (32) as,

$$\mathbf{F}_{\xi|\xi} = \left(\frac{\partial \boldsymbol{\epsilon}(\boldsymbol{\xi})}{\partial \boldsymbol{\xi}^T}\right)^T \mathbf{F}_{\boldsymbol{\epsilon}|\boldsymbol{\epsilon}} \frac{\partial \boldsymbol{\epsilon}(\boldsymbol{\xi})}{\partial \boldsymbol{\xi}^T} = \begin{bmatrix} F_{\sigma_n^2|\xi}(\boldsymbol{\xi}) & \mathbf{0} & \mathbf{0} \\ \mathbf{0} & \mathbf{F}_{\boldsymbol{\theta}_0|\xi}(\boldsymbol{\xi}) & \mathbf{F}_{\boldsymbol{\theta}_0,\tau_1,\rho_1,\phi_1|\xi}(\boldsymbol{\xi}) \\ \mathbf{0} & \mathbf{F}_{\tau_1,\rho_1,\phi_1,\theta_0|\xi}(\boldsymbol{\xi}) & \mathbf{F}_{\tau_1,\rho_1,\phi_1|\xi}(\boldsymbol{\xi}) \end{bmatrix}. \tag{A44}$$

with

$$F_{\sigma_n^2|\xi}(\boldsymbol{\xi}) = F_{\sigma_n^2|\boldsymbol{\epsilon}}(\boldsymbol{\epsilon}), \tag{A45}$$

$$\mathbf{F}_{\boldsymbol{\theta}_0|\xi}(\boldsymbol{\xi}) = \mathbf{F}_{\boldsymbol{\theta}_0|\boldsymbol{\epsilon}}(\boldsymbol{\epsilon}) + \mathbf{E}_1\mathbf{F}_{\boldsymbol{\theta}_1|\boldsymbol{\epsilon}}(\boldsymbol{\epsilon})\mathbf{E}_1 + \mathbf{E}_1\mathbf{F}_{\boldsymbol{\theta}_1,\boldsymbol{\theta}_0|\boldsymbol{\epsilon}}(\boldsymbol{\epsilon}) + \mathbf{F}_{\boldsymbol{\theta}_0,\boldsymbol{\theta}_1|\boldsymbol{\epsilon}}(\boldsymbol{\epsilon})\mathbf{E}_1, \tag{A46}$$

$$\mathbf{F}_{\tau_1,\rho_1,\phi_1|\xi}(\boldsymbol{\xi}) = \mathbf{E}_3^T\mathbf{F}_{\boldsymbol{\theta}_1|\boldsymbol{\epsilon}}(\boldsymbol{\epsilon})\mathbf{E}_3, \tag{A47}$$

$$\mathbf{F}_{\tau_1,\rho_1,\phi_1,\boldsymbol{\theta}_0|\xi}(\boldsymbol{\xi}) = \left(\mathbf{F}_{\boldsymbol{\theta}_0,\tau_1,\rho_1,\phi_1|\xi}(\boldsymbol{\xi})\right)^T = \mathbf{E}_3^T\mathbf{F}_{\boldsymbol{\theta}_1,\boldsymbol{\theta}_0|\boldsymbol{\epsilon}}(\boldsymbol{\epsilon}) + \mathbf{E}_3^T\mathbf{F}_{\boldsymbol{\theta}_1|\boldsymbol{\epsilon}}(\boldsymbol{\epsilon})\mathbf{E}_1. \tag{A48}$$

The constrained FIM can directly be computed using the (10) and (13). Besides, the expression of $\mathbf{W}^{\Delta}$ components is simplified by the assumption $b_0 = b_1$ as follows,

$$
\begin{aligned}
&W^{\Delta}_{1,1} = \frac{1}{F_s}\mathbf{s}^H\mathbf{V}^{\Delta,0}\left(\frac{\Delta\tau}{T_s}\right)\mathbf{s},\ W^{\Delta}_{1,2} = \frac{1}{F_s^2}\mathbf{s}^H\mathbf{D}\mathbf{V}^{\Delta,0}\left(\frac{\Delta\tau}{T_s}\right)\mathbf{s},\ W^{\Delta}_{1,3} = -\mathbf{s}^H\mathbf{V}^{\Delta,1}\left(\frac{\Delta\tau}{T_s}\right)\mathbf{s},\\
&W^{\Delta}_{2,1} = \frac{1}{F_s^2}\mathbf{s}^H\mathbf{V}^{\Delta,0}\left(\frac{\Delta\tau}{T_s}\right)\mathbf{D}\mathbf{s},\ W^{\Delta}_{2,2} = \frac{1}{F_s^3}\mathbf{s}^H\mathbf{D}\mathbf{V}^{\Delta,0}\left(\frac{\Delta\tau}{T_s}\right)\mathbf{D}\mathbf{s},\ W^{\Delta}_{2,3} = -\frac{1}{F_s}\mathbf{s}^H\mathbf{V}^{\Delta,1}\left(\frac{\Delta\tau}{T_s}\right)\mathbf{D}\mathbf{s},\\
&W^{\Delta}_{3,1} = \mathbf{s}^H\mathbf{V}^{\Delta,1}\left(\frac{\Delta\tau}{T_s}\right)\mathbf{s},\ W^{\Delta}_{3,2} = \frac{1}{F_s}\mathbf{s}^H\mathbf{D}\mathbf{V}^{\Delta,1}\left(\frac{\Delta\tau}{T_s}\right)\mathbf{s},\ W^{\Delta}_{3,3} = F_s\mathbf{s}^H\mathbf{V}^{\Delta,2}\left(\frac{\Delta\tau}{T_s}\right)\mathbf{s}.
\end{aligned}
\tag{A49}
$$

References

1. Van Trees, H.L. Part III: Radar-Sonar Signal Processing and Gaussian Signals in Noise. In *Detection, Estimation, and Modulation Theory*; John Wiley & Sons: Hoboken, NJ, USA, 2001.
2. Chen, J.; Huang, Y.; Benesty, J. Time Delay Estimation. In *Audio Signal Processing for Next-Generation Multimedia Communication Systems*; Huang, Y., Benesty, J., Eds.; Springer: Boston, MA, USA, 2004; Chapter 8, pp. 197–227.
3. Levy, B.C. *Principles of Signal Detection and Parameter Estimation*; Springer: Berlin/Heidelberg, Germany, 2008.
4. Mengali, U.; D'Andrea, A.N. *Synchronization Techniques for Digital Receivers*; Plenum Press: New York, NY, USA, 1997.
5. Fernández-Prades, C.; Lo Presti, L.; Falletti, E. Satellite radiolocalization from GPS to GNSS and beyond: novel technologies and applications for civil mass market. *Proc. IEEE* **2011**, *99*, 1882–1904. [CrossRef]
6. Amin, M.G.; Closas, P.; Broumandan, A.; Volakis, J.L. Vulnerabilities, Threats, and Authentication in Satellite-based Navigation Systems [scanning the issue]. *Proc. IEEE* **2016**, *104*, 1169–1173. [CrossRef]
7. Zavorotny, V.U.; Gleason, S.; Cardellach, E.; Camps, A. Tutorial on remote sensing using GNSS bistatic radar of opportunity. *IEEE Geosci. Remote Sens. Mag.* **2014**, *2*, 8–45. [CrossRef]
8. Townsend, B.R.; Fenton, P.C.; Van Dierendonck, K.J.; Richard Van Nee, D.J. Performance Evaluation of the Multipath Estimating Delay Lock Loop. *Navigation* **1995**, *42*, 502–514. [CrossRef]
9. Weill, L.R. Multipath Mitigation using Modernized GPS Signals: How Good Can it Get? In Proceedings of the 15th International Technical Meeting of the Satellite Division of The Institute of Navigation (ION GPS 2002), Portland, OR, USA, 24–27 September 2002; pp. 493–505.
10. Fenton, P.C.; Jones, J. The Theory and Performance of NovAtel Inc.'s Vision Correlator. In Proceedings of the 18th International Technical Meeting of the Satellite Division of The Institute of Navigation, Long Beach, CA, USA, 13–16 September 2005; pp. 2178–2186.
11. Lowe, S.T.; LaBrecque, J.L.; Zuffada, C.; Romans, L.J.; Young, L.E.; Hajj, G.A. First Spaceborne Observation of an Earth-reflected GPS Signal. *Radio Sci.* **2002**, *37*, 1–28. [CrossRef]
12. Lestarquit, L.; Peyrezabes, M.; Darrozes, J.; Motte, E.; Roussel, N.; Wautelet, G.; Frappart, F.; Ramillien, G.; Biancale, R.; Zribi, M. Reflectometry with an Open-Source Software GNSS Receiver: Use Case with Carrier Phase Altimetry. *IEEE J. Sel. Top. Appl. Earth Obs. Remote Sens.* **2016**, *9*, 4843–4853. [CrossRef]
13. Treuhaft, R.; Lowe, S.; Zuffada, C.; Chao, Y. 2-cm GPS Altimetry over Crater Lake. *Geophys. Res. Lett.* **2001**, *22*, 4343–4346. [CrossRef]
14. Zavorotny, V.U.; Larson, K.M.; Braun, J.J.; Small, E.E.; Gutmann, E.D.; Bilich, A.L. A Physical Model for GPS Multipath Caused by Land Reflections: Toward Bare Soil Moisture Retrievals. *IEEE J. Sel. Top. Appl. Earth Obs. Remote Sens.* **2010**, *3*, 100–110. [CrossRef]
15. Dogandzic, A.; Nehorai, A. Cramer-Rao Bounds for Estimating Range, Velocity, and Direction with an Active Array. *IEEE Trans. Signal Process.* **2001**, *49*, 1122–1137. [CrossRef]
16. Das, P.; Vilà-Valls, J.; Chaumette, E.; Vincent, F.; Davain, L.; Bonnabel, S. On the Accuracy Limit of Time-delay Estimation with a Band-limited Signal. In Proceedings of the ICASSP 2019—2019 IEEE International Conference on Acoustics, Speech and Signal Processing (ICASSP), Brighton, UK, 12–17 May 2019; pp. 5282–5286.
17. Medina, D.; Ortega, L.; Vilà-Valls, J.; Closas, P.; Vincent, F.; Chaumette, E. A New Compact CRB for Delay, Doppler and Phase Estimation—Application to GNSS SPP & RTK Performance Characterization. *IET Radar Sonar Navig.* **2020**. [CrossRef]

18. Das, P.; Vilà-Valls, J.; Vincent, F.; Davain, L.; Chaumette, E. A New Compact Delay, Doppler Stretch and Phase Estimation CRB with a Band-Limited Signal for Generic Remote Sensing Applications. *Remote Sens.* **2020**, *12*, 2913. [CrossRef]
19. Bartov, A.; Messer, H. Lower Bound on the Achievable DSP Performance for Localizing Step-Like Continuous Signals in Noise. *IEEE Trans. Signal Process.* **1998**, *46*, 2195–2201. [CrossRef]
20. Ricker, D.W. *Echo Signal Processing*; Kluwer Academic; Springer: New York, NY, USA, 2003.
21. Kay, S.M. *Fundamentals of Statistical Signal Processing: Estimation Theory*; Prentice-Hall: Englewood Cliffs, NJ, USA, 1993.
22. Ottersten, B.; Viberg, M.; Stoica, P.; Nehorai, A. Exact and Large Sample Maximum Likelihood Techniques for Parameter Estimation and Detection in Array Processing. In *Radar Array Processing*; Haykin, S., Litva, J., Shepherd, T.J., Eds.; Springer: Heidelberg, Germany, 1993; Chapter 4, pp. 99–151.
23. Yau, S.F.; Bresler, Y. A Compact Cramér-Rao Bound Expression for Parametric Estimation of Superimposed Signals. *IEEE Trans. Signal Process.* **1992**, *40*, 1226–1230. [CrossRef]
24. Menni, T.; Chaumette, E.; Larzabal, P. Reparameterization and Constraints for CRB: Duality and a Major Inequality for System Analysis and Design in the Asymptotic Region. In Proceedings of the 2012 IEEE International Conference on Acoustics, Speech and Signal Processing (ICASSP), Kyoto, Japan, 25–30 March 2012; pp. 3545–3548.
25. Zhao, T.; Huang, T. Cramer-Rao Lower Bounds for the Joint Delay-Doppler Estimation of an Extended Target. *IEEE Trans. Signal Process.* **2016**, *64*, 1562–1573. [CrossRef]
26. Germain, O.; Ruffini, G. A Revisit to the GNSS-R Code Range Precision. *arXiv* **2006**, arXiv:0606180.
27. Camps, A.; Park, H.; Valencia i Domènech, E.; Pascual, D.; Martin, F.; Rius, A.; Ribo, S.; Benito, J.; Andrés-Beivide, A.; Saameno, P.; et al. Optimization and Performance Analysis of Interferometric GNSS-R Altimeters: Application to the PARIS IoD Mission. *IEEE J. Sel. Top. Appl. Earth Obs. Remote Sens.* **2014**, *7*, 1436–1451. [CrossRef]
28. Ribot, M.A.; Botteron, C.; Farine, P. Derivation of the Cramér-Rao Bound in the GNSS-Reflectometry Context for Static, Ground-Based Receivers in Scenarios with Coherent Reflection. *Sensors* **2016**, *16*, 2063. [CrossRef]
29. Stoica, P.; Nehorai, A. Performances Study of Conditional and Unconditional Direction of Arrival Estimation. *IEEE Trans. Acoust. Speech Signal Process.* **1990**, *38*, 1783–1795. [CrossRef]
30. Menni, T.; Chaumette, E.; Larzabal, P.; Barbot, J.P. CRB for Active Radar. In Proceedings of the 2011 19th European Signal Processing Conference, Barcelona, Spain, 29 August–2 September 2011.
31. Menni, T.; Galy, J.; Chaumette, E.; Larzabal, P. Versatility of Constrained CRB for System Analysis and Design. *IEEE Trans. Aerosp. Electron. Syst.* **2014**, *50*, 1841–1863. [CrossRef]
32. Vincent, F.; Besson, O.; Chaumette, E. Approximate Maximum Likelihood Direction of Arrival Estimation for Two Closely Spaced Sources. In Proceedings of the 2013 5th IEEE International Workshop on Computational Advances in Multi-Sensor Adaptive Processing (CAMSAP), St. Martin, France, 15–18 December 2013; pp. 320–323.
33. Vincent, F.; Besson, O.; Chaumette, E. Approximate Maximum Likelihood Estimation of Two Closely Spaced Sources. *Signal Process.* **2014**, *97*, 83–90. [CrossRef]
34. Renaux, A.; Forster, P.; Chaumette, E.; Larzabal, P. On the High-SNR Conditional Maximum-Likelihood Estimator Full Statistical Characterization. *IEEE Trans. Signal Process.* **2006**, *54*, 4840–4843. [CrossRef]
35. Ortega, L.; Medina, D.; Vilà-Valls, J.; Vincent, F.; Chaumette, E. Positioning Performance Limits of GNSS Meta-Signals and HO-BOC Signals. *Sensors* **2020**, *20*, 3586. [CrossRef] [PubMed]
36. Capon, J. High-Resolution Frequency-Wavenumber Spectrum Analysis. *Proc. IEEE* **1969**, *57*, 1408–1418. [CrossRef]
37. Schmidt, R.O. Multiple Emitter Location and Signal Parameter Estimation. *IEEE Trans. Antennas Propag.* **1986**, *34*, 276–280. [CrossRef]
38. Stoica, P.; Nehorai, A. MUSIC, Maximum Likelihood and Cramer-Rao Bound. In Proceedings of the International Conference on Acoustics, Speech, and Signal Processing (ICASSP-88), New York, NY, USA, 11–14 April 1988; Volume 4, pp. 2296–2299.
39. Ziskind, I.; Wax, M. Maximum Likelihood Localization of Multiple Sources by Alternating Projection. *IEEE Trans. Acoust. Speech Signal Process.* **1988**, *36*, 1553–1560. [CrossRef]
40. Li, J.; Stoica, P. Efficient mixed-spectrum estimation with applications to target feature extraction. *IEEE Trans. Signal Process.* **1996**, *44*, 281–295.

41. Beckmann, P.; Spizzichino, A. *The Scattering of Electromagnetic Waves From Rough Surfaces*; Artech House: Norwood, MA, USA, 1987.
42. Kaplan, E.; Hegarty, C. (Eds.) *Understanding GPS: Principles and Applications*, 2nd ed.; Artech House: Norwood, MA, USA, 2006.
43. Van Trees, H.L. Part I: Detection Estimation and Linear Modulation Theory. In *Detection, Estimation, and Modulation Theory*; John Wiley & Sons: Hoboken, NJ, USA, 2001.
44. Das, P.; Ortega, L.; Vilà-Valls, J.; Vincent, F.; Chaumette, E.; Davain, L. Performance Limits of GNSS Code-Based Precise Positioning: GPS, Galileo & Meta-Signals. *Sensors* **2020**, *20*, 2196. [CrossRef]
45. U.S. Goverment. Interface Specification IS-GPS-200 Navstar GPS Space/Segment/Navigation User Interface. Available online: https://www.gps.gov/technical/icwg/IS-GPS-200K.pdf (accessed on 16 January 2020).
46. Lehmann, E.L.; Casella, G. *Theory of Point Estimation*, 2nd ed.; Springer: New York, NY, USA, 1998.
47. Hu, C.; Benson, C.; Park, H.; Camps, A.; Qiao, L.; Rizos, C. Detecting Targets above the Earth's Surface Using GNSS-R Delay Doppler Maps: Results from TDS-1. *Remote Sens.* **2019**, *11*, 2327. [CrossRef]